



Zhang, Z., Park, J., Kwon, O-S., Sextos, A., Strepelias, E., Stathas, N., & Bousias, S. (2020). Hybrid Simulation of a Structure-Pipe-Structure Interaction Within a Gas Processing Plant. *Journal of Pipeline Systems Engineering and Practice*, 12(2).
[https://doi.org/10.1061/\(ASCE\)PS.1949-1204.0000526](https://doi.org/10.1061/(ASCE)PS.1949-1204.0000526)

Peer reviewed version

Link to published version (if available):
[10.1061/\(ASCE\)PS.1949-1204.0000526](https://doi.org/10.1061/(ASCE)PS.1949-1204.0000526)

[Link to publication record in Explore Bristol Research](#)
PDF-document

This is the author accepted manuscript (AAM). The final published version (version of record) is available online via American Society of Civil Engineers at [https://doi.org/10.1061/\(ASCE\)PS.1949-1204.0000526](https://doi.org/10.1061/(ASCE)PS.1949-1204.0000526) . Please refer to any applicable terms of use of the publisher.

University of Bristol - Explore Bristol Research

General rights

This document is made available in accordance with publisher policies. Please cite only the published version using the reference above. Full terms of use are available:
<http://www.bristol.ac.uk/red/research-policy/pure/user-guides/ebr-terms/>

HYBRID SIMULATION OF STRUCTURE-PIPE-STRUCTURE INTERACTION WITHIN A GAS PROCESSING PLANT

Ziliang Zhang¹, Jamin Park, Ph.D.², Oh-Sung Kwon, Ph.D., P.Eng., M.ASCE³, Anastasios Sextos, Ph.D., M.ASCE⁴,
Elias Strepelias, Ph.D.⁵, Nikolaos Stathas, Ph.D.⁶, and Stathis Bousias, Ph.D.⁷

¹Ph.D. Candidate, Dept. of Civil Engineering, Univ. of Bristol, Queen's Bldg., University Walk, Bristol BS8 1TR,
UK. Email: zz17635@bristol.ac.uk

²Postdoctoral Research Fellow, Dept. of Civil and Mineral Engineering, Univ. of Toronto, Toronto, ON, Canada M5S
1A4. Email: jamin.park@utoronto.ca

³Professor, Dept. of Civil and Mineral Engineering, Univ. of Toronto, Toronto, ON, Canada M5S 1A4. Email:
os.kwon@utoronto.ca

⁴Professor, Dept. of Civil Engineering, Univ. of Bristol, Queen's Bldg., University Walk, Bristol BS8 1TR, UK
(corresponding author). Email: a.sextos@bristol.ac.uk

⁵Postdoctoral Research Fellow, Structures Laboratory, Dept. of Civil Engineering, Univ. of Patras, Patras 26504,
Greece. E-mail: ilstrepelias@upatras.gr

⁶Postdoctoral Research Fellow, Structures Laboratory, Dept. of Civil Engineering, Univ. of Patras, Patras 26504,
Greece. E-mail: stathas@upatras.gr

⁷Professor, Director of Structures Laboratory, Dept. of Civil Engineering, Univ. of Patras, Patras 26504, Greece.
E-mail: sbousias@upatras.gr

ABSTRACT

Though often overlooked, the impact of seismic transient ground deformation on natural gas (NG) pipes can be highly adverse. Particularly, pipe elbows may undergo excessive in-plane bending demand and buckling. In this paper, a critical scenario of a pipe coupling two industrial structures typically found in an NG processing plant is studied. High strain and cross-sectional ovalization on the elbows are probable during an earthquake due to the out-of-phase oscillation of the two structures imposing asynchronous displacement demands at the two pipe-ends. A parametric study was first performed to investigate various structure-pipe-structure configurations which increase seismic demands to pipe elbows. Simultaneous mobilisation of divergent oscillation between two supporting structures at the low-frequency range, a lower pipe-structure stiffness ratio, a shorter length of straight pipe segments in the linking pipe element and a higher pipe internal pressure have led to the onset of critical strain demands in pipe elbows. To validate this observation, an experimental campaign was developed where a full-scale linking pipe element was

30 physically tested by means of hybrid simulation (HS). The study shows that the seismic interaction of the structures
31 coupled with the pipe is non-negligible and can be even critical for the integrity of the coupling pipe. The finding
32 depends on the structural system's dynamic and geometrical properties as well the frequency content of the earthquake
33 excitation.

34 INTRODUCTION

35 Natural gas (NG) constitutes a significant percentage of nowadays global energy consumption. Its demand has
36 increased over the past decade and is expected to proliferate into the future with increased global interest in clean energy
37 (U.S. Department of Energy 2017; Sextos et al. 2018). Among many factors, transport and supply play an essential role
38 in the NG industry, which includes transmission, storage, gas liquefaction and regasification (GIE 2015). Since NG
39 reserves are commonly distant from consumer markets, the need for delivering NG to end-users has led to the world's
40 mass construction of complex lifeline systems with numerous integrated components and processes. In 2019, the annual
41 regasification capacity of large-scale liquefied natural gas (LNG) terminals in Europe came to 241 billion $m^3(N)/year$
42 and capacity expansion of another 140 billion $m^3(N)/year$ was planned (GIE 2019). Along with its clear economic
43 and strategic importance, NG facilities are often associated with high natural and man-made risks. As a result, gas
44 infrastructure security and safety has always been the core value of NG transmission facilities such as LNG terminals,
45 compression stations, peak sheaving stations, pressure let-down stations, and blending stations, which are vulnerable
46 to natural hazards, such as earthquakes. In the last decade, natural hazard triggering technological accidents (Na-Tech),
47 and more specifically seismic Na-Tech, has been slowly accepted as a fundamental contribution to the overall risk
48 assessment figures calculated by considering solely industrial accidents (Lanzano et al. 2015). Past Na-Tech disasters
49 have displayed such devastating consequences in causing substantial social, economic and environmental loss that
50 the future prevention of loss of containment events in critical infrastructures is clearly an issue of major importance
51 (Nakashima et al. 2014).

52 Pipe elbows are critical components to the safety of pipe within NG processing plants. Compared to straight
53 pipe segments with the identical cross-section specification and material properties, the elbows are more flexible and
54 associated with significantly higher stresses, strains and cross-sectional ovalization (Karamanos 2016). To date, code
55 prescriptions of seismic design for pipelines are generally scarce. In Eurocode 8, for example, principal guidelines were
56 provided for above-ground pipeline in accordance with generic seismic design approaches (CEN 2006). In terms of
57 research, much effort has been devoted on dynamic analysis of above-ground pipe elbows, mostly in the form of cyclic
58 bending analysis of individual elbow members where their failure mode under extreme loading conditions were heavily
59 investigated both numerically and experimentally. The most-reported elbow damage pattern was the axial development
60 of through-wall cracks near elbow flanks due to low cycle fatigue accompanied by ratcheting effect (Hasegawa et al.
61 2008; Hassan et al. 2015; Jeon et al. 2017; Karvelas et al. 2019; Nakamura and Kasahara 2016; Nakamura and Kasahara

2017; Varelis et al. 2012; Watakabe et al. 2017), while evidence of local buckling followed by crack development has also been mentioned (Hasegawa et al. 2008).

Investigations also went into complex pipe systems coupled within industrial structures and plants. Reza et al. (2013) investigated, by means of HS, the seismic performance of a full-scale pipe system coupled within a single industrial building. The pipe system is located on the top-level of a 3-storey steel structure and is connected to a number of storage tanks and devices inside the structure. Test results showed that even with the maximum earthquake input under their investigation, the pipeline system remained below the yield limit at all locations. The authors of this paper believed that excessive strain development on pipe was inhibited because all supporting points of the pipe was contained on the same floor of the same structure, which is likely to respond synchronously during the earthquake. We stress that this would not necessarily be the case if different support points of the pipe (in a single structure or between multiple structures, or between a structure and the free field) vibrated out-of-phase.

For above-ground pipes, Sakai et al. (2013) evaluated the safety of a piping system using HS, where a 90-degree elbow was physically tested and the remainder of the pipeline system was simulated in a coupled numerical model. Permitted the assumption that one end of the elbow specimen was fully fixed onto the laboratory floor and therefore had zero motion, the test concluded that the 8-inch diameter uniform wall-thinning elbow can fail in the form of low cyclic fatigue under certain conditions. Vathi et al. (2017) simulated the seismic performance of a pipe system and its associated pipe rack and liquid storage tank within an industrial plant. Underwent seismic excitation, it was found that the critical component of the pipe system was the upper elbow located at the top of a pipe rack, where local strain value exceeded the limit of severe plasticization. The differential motion between the ground surface and the structural response on top of the pipe rack where the pipe was elevated, made it possible the asynchronous displacements at two ends of the elbow hence the conspicuous elbow in-plane bending. Sextos et al. (2017) examined numerically the seismic performance of mechanical sub-systems within a nuclear power plant containment structure using refined finite element models. It was found that under certain circumstances, elbows were susceptible to significantly increased seismic demand if geometrical nonlinearities introduced by the effects of structure rocking and sliding with uplift are considered. Wenzel et al. (2018) analysed the nonlinear behaviour of a coupled foundation-tank-pipeline system using HS, where a liquid storage tank and its base-isolated foundation were simulated numerically and a small portion of pipe connected directly to the tank was tested physically. Under the assumption that the far-end of the physical pipe specimen was fully fixed to the laboratory floor, a significant displacement time history was exerted onto the physical pipe specimen during the HS. The result showed that the critical component was one of the elbows located near heavy auxiliary masses on pipe. Bursi et al. (2018) numerically evaluated the nonlinear response of a whole LNG plant under moderate seismic loading. The study found elbows on top of the tall LNG storage tank were the critical components in the loop and can exhibit high degree of vulnerability during transient ground motions. This was because of the high differential displacement between the pipe rack and the pump columns located over the dome of the storage tank.

95 Similarly, for buried NG pipelines, the impact of out-of-phase oscillation induced by differential earthquake inputs
96 has been highlighted previously. Psyrras et al. numerically (2019) and experimentally (2020) investigated the seismic
97 risk of buried NG pipelines when subjected to spatially varying transient ground deformations. Results showed that
98 even for straight buried pipelines, the seismic vibrations at the vicinity of laterally inhomogeneous sites can produce
99 differential movements on different locations of a long pipeline due to kinematic soil-pipe interaction. As a result,
100 appreciable axial stress concentration can be observed in the critically affected pipeline segment near the soil material
101 discontinuity, high enough to trigger coupled buckling modes into the plastic range.

102 Notwithstanding the above advancements there are still several clear limitations in the existing literature. While
103 many studies investigate the seismic demand of pipe coupled to its surroundings, rarely had a set of realistic boundary
104 conditions been successfully adopted to a realistic seismic scenario where differential displacement between the two
105 pipe-ends of an above-ground pipe was significant. It was not uncommon in previous studies that researchers employed
106 overbold assumptions regarding boundary conditions of the pipe supports, such as full constraint (zero motion) at
107 one end of the investigated pipe, whereas in reality any pipe support connected to another entity should have the
108 corresponding motion at the boundary. For example, the base of a pipe support anchored onto the ground surface
109 would be subjected to the same excitation as the foundation input motion exerted to nearby structures. This level of
110 boundary condition accuracy is the bare-minimum that should be adopted in any modelling practices of above-ground
111 pipes, regardless of considering or neglecting any potential coupling effect. Further more, the importance of structure
112 coupling in industrial NG plants due to the existence of pipes extending between them has not yet been addressed. It
113 is unclear that to what extent the negligence of structural coupling introduced by bridging NG pipes can affect their
114 design prospect. Should the interaction leads to detrimental effects, whether buckling failure or other forms of damage
115 can occur on the pipes or the coupled structures during transient ground motion awaits investigation. Finally, how the
116 coupling effect is influenced by the various properties of the pipe and those of the supporting industrial structures, as
117 well as the characteristic of the input earthquake excitation remains in doubt.

118 Along these lines, the objectives of this paper are:

- 119 • to identify key parameters of the coupling problem within the proposed structure-pipe-structure configuration,
120 illustrate the sensitivity of both the global structural response and the induced local elbow demand to these
121 parameters and their most critical combination, by means of finite element analysis (FEA).
- 122 • to experimentally examine the damage potential of pipe when it is subjected to the differential displacement be-
123 tween two pipe-ends by means of hybrid simulation (HS), given that the difficulties associated with numerically
124 modelling geometrical nonlinearities of pressurised pipe with buckling potential, the effect of non-negligible
125 structure-pipe-structure interaction and the scale of the industrial structures involved in the proposed scenario.

PROBLEM STUDIED

The scenario examined herein consists of two realistic industrial building configurations: supporting structure A is a three-storey NG compressor house, supporting structure B is an exposed platform topped with two tall and heavy reliquefaction condensers on its deck (Fig.1, a). Both structures are steel moment-resisting frames with reinforced concrete slabs and are assumed to behave elastically. They have first-mode natural frequencies of $f_A = 3.3$ Hz and $f_B = 2.3$ Hz, respectively, hence a structural frequency ratio is $f_B/f_A = 0.7$. There is an NG pipe behaving as a linking element between the two structures with a cross-sectional diameter of 219.6 mm, wall-thickness of 6.3 mm and two 90-degree elbows with bend radius of 302.0 mm located in the middle. The elbow bend factor is therefore $h = Rt/(D/2)^2 = 0.16$. The two structures are laterally separated at a perpendicular distance of 7.56 m and the length of the intermediate straight pipe segment between two 90-degree elbows is 1.38 m. A slender steel column supports the pipe near the middle, providing merely vertical resistance. As the overall pipe-structure system is subjected to ground excitation alone x-axis, differential displacement between the two pipe-ends imposes compression or tension to the bridging pipe as the two supporting structures vibrate out-of-phase, bending the pipe elbows in-plane. This is the result of different dynamic responses of the two structures even though the earthquake ground motion they were subjected to is actually identical given their short separating distance and the common foundation and underlying soil profile.

Existing design criteria require that for the case where a secondary system is attached to a primary system, the evaluation of the coupling effect can only be neglected if the total mass of the interacting secondary system is less than 1% of the primary supporting structure (Fouquiau et al. 2018; Taghavi and Miranda 2008). However, it has also been pointed out that if the secondary system is extended and is supported at two or more locations, the coupling effect shall be investigated regardless of any mass percentage value (Firoozabad et al. 2015). The authors believe cautiousness is even more indispensable for the structure-pipe-structure configuration proposed herein, where the secondary system, i.e. the linking NG pipe, is attached to two dynamic systems with divergent dynamic characteristics and is therefore excited by the out-of-phase oscillation between the latter. Fundamentally, if a decoupled analysis is to be carried out for a partial structure, it is vital to ensure that the decoupling does not significantly affect the frequencies and the response of the primary system (Gupta and Tembulkar 1984). From preliminary numerical analyses of the proposed structure-pipe-structure system, it was observed that while the natural frequencies of the two structures were not altered dramatically by the presence or removal of the linking pipe element, a clear deviation of the structural response between the holistic case and the no-pipe case was noted; thus, coupled analysis for the proposed scenario is appropriate and necessary.

IDENTIFICATION OF KEY PROBLEM PARAMETERS AND MAXIMUM PIPE DEMAND

Analysis Outline

For an in-depth study of the problem and to find realistic conditions under which the seismic demand on the pipe becomes critical, a parametric analysis scheme was established using the general-purpose finite element analysis software ABAQUS (Dassault Systèmes Simulia Corp. 2014). To parameterize the proposed structure-pipe-structure scenario, the two supporting structures were simplified to equivalent SDOF oscillators topped with lumped mass (Fig. 1, b). Due to the fact that the emphasis of the structure-pipe-structure scenario investigated herein is on the eventual damage of pipe elbows when the linking pipe element is subjected to differential displacement between its two ends, the equivalent SDOF oscillators were assumed to behave linear elastically and were modelled using the ABAQUS Two-node Linear Beam In Space Element, B31. The simplification preserved the elevation of the pipe anchor point, the first-mode natural frequency of the structures, the elastic swaying stiffness of the structures and the structural mass concentrated at the elevation of gravity centre of the corresponding detailed 3D models. Further more, given that the prototypes of the two supporting structures are moment resisting frames with axially stiff slab, which are expected to deform in shear during earthquakes, the stiff structure floors onto which the linking pipe are extended and attached are assumed parallel to the flat ground surface throughout the duration of ground excitation. Therefore, the two pipe-ends in the simplified model were fixed to the oscillator at first five degree-of-freedom (DOF) and were free on the sixth DOF, i.e. rotation about z-axis. Note that the simplified pipe connection may introduce a certain degree of error in terms of the state of strain on pipe, as demonstrated by Guarracino et al. (2009) both numerically and experimentally for a four-point bent pipe. It was also assumed that the ground excitation is limited to x-axis-only and that the vibration of the equivalent SDOF supporting structures were restricted in the xy-plane, which is the vibration direction of the dominant first-mode response of the corresponding detailed 3D models. Finally, we assumed that the base of the two equivalent SDOF supporting structures were fully fixed to the ground and were always subjected to the identical input ground excitation. On the other hand, the linking pipe was modelled in a greater detail to capture its potential buckling and nonlinear hysteretic response under dynamic loading. The ABAQUS Four-node Reduced-Integration Shell Element, S4R, was utilised for modelling the pipe geometry, assigning plastic material properties with a linear kinematic hardening rule. The mesh density on the elbows was set to 54 elements around the cylinder circumference and 3510 shell elements in total for each 90-degree elbows. Coarser mesh was chosen for the straight pipe segments as the excessive strain development and nonlinearities are expected to concentrate on and around the elbows. The selected type and size of shell element have been widely used in previous pipe elbow modelling practices (Varelis et al. 2011; Vazouras et al. 2010) and were proven reliable through our preliminary analyses. To verify the model simplifications, we define $D_{diff}(t)$ as the time history of x-directional differential displacement between the two pipe-ends (Eq. 1):

$$D_{diff}(t) = u_B(t) - u_A(t) \quad (1)$$

where $u_A(t), u_B(t)$ are the time variation of x-axis positions of pipe-end points A and B. Validation of the equivalent SDOF simplification in its ability of reliably reproducing the structural displacement responses was demonstrated by a comparison of $D_{diff}(t)$ results between a detailed 3D model as shown in Fig.1, a and a simplified model as shown in Fig.1, b. The $D_{diff}(t)$ result produced by the simplified model using equivalent SDOF oscillators compared well with the corresponding $D_{diff}(t)$ obtained from detailed 3D model.

The parameters examined in the numerical parametric study are identified in Table 1. In particular, f_B/f_A is the ratio of the first-mode natural frequencies of structure B and A, respectively. The parameter f_g is the predominant frequency of input excitation, determined at the frequency where the highest peak occurs in its Fast Fourier Transform diagram. They jointly describe the fundamental dynamic mechanism of the out-of-phase oscillation between the two supporting structures. Parameter H_p aims to capture the amplification of pipe-end differential displacement due to higher pipe elevation given the same structure, pipe and excitation properties. The influence of pipe-structure stiffness ratio is also examined through the reflecting variable of linear elastic equivalent SDOF swaying stiffnesses of the two supporting structures K_A, K_B . The length of the straight pipe segment between the two 90-degree elbows L_z and the perpendicular distance between the two supporting structures L_x are further varied to assess the impact of different geometry of the structure-pipe-structure configuration. Finally, internal pressure of the NG pipe P is examined to consider the different operation conditions of a pressurised NG pipe. Other parameters, including pipe cross-sectional specifications, the geometry of the pipe elbows, pipe material properties, structural damping ratio, structure shape characterised by the elevation of its mass centre and the peak ground acceleration (PGA) of the input excitation, are taken as constants as the impacts of their variations are not unique for the problem presented herein.

The value of variables in the reference FE model is summarised herein as well as in Fig.1, a. It has structural frequencies $f_A = 2.2$ Hz and $f_B = 3.3$ Hz, hence $f_B/f_A = 0.7$. The input ground motion is selected from the 1972 Nicaragua earthquake recorded at Managua ESSO station, with a predominant frequency $f_g = 2.2$ Hz (Input motion 4 in Fig.4). The equivalent SDOF swaying stiffness of the supporting structures are $K_A = 52670$ kN/m and $K_B = 16670$ kN/m. Given the natural frequency and the stiffness, the mass of the two supporting structures in the reference case are $M_A = 122.5$ tonne and $M_B = 79.8$ tonne, respectively. The geometry of the structure-pipe-structure system is described with the parameters $H_p = 5.30$ m, $L_z = 1.38$ m and $L_x = 7.56$ m. The pipe internal pressure is $P = 3.0$ MPa. Note that in each of the following variations in the parametric study, only the examined parameter(s) will be deviated from the reference case in each section.

Structural and pipe response quantities examined throughout the parametric study are $D_{diff,max}$ and $\epsilon_{h,max}$. The peak differential displacement between two pipe-ends, $D_{diff,max}$, is defined as the absolute value of the largest in time pipe-end differential displacement $D_{diff}(t)$ occurred during the excitation:

$$D_{diff,max} = \max(|D_{diff}(t)|), \quad t = 0 \rightarrow t_g \quad (2)$$

where t_g is the total length of the input ground excitation. $D_{diff,max}$ is therefore a non-negative scalar derived for each analysis case, providing insight into the level of global response of the coupled structure-pipe-structure dynamic system. Similarly, the maximum hoop strain on the elbows, $\epsilon_{h,max}$, defined as the largest amplitude of elbow hoop strain $\epsilon_h(t)$ obtained during the excitation within the 90-degree bent elbows, represents the level of local seismic elbow strain demand. Like any peak values, the $D_{diff,max}$ and the $\epsilon_{h,max}$ neither reflect the time variation nor the potential cumulative character of the response quantities. Nonetheless, as scalars, they provide straightforward indications of the level of seismic demand to the pipe and can be comprehended within the context of parametric study.

Effect of Structural and Ground Motion Frequencies

To gain understanding into the frequency-dependency of the peak differential displacement between two pipe-ends $D_{diff,max}$ and the induced maximum elbow hoop strain $\epsilon_{h,max}$, we examine the ratio of first-mode natural frequencies of the two supporting structures f_B/f_A and the frequency content of the input excitation characterised by its predominant frequency f_g . Given that the purpose of the study was not to explore fatigue or ground motion duration impact on nonlinear response of the elbows, but to identify the effect of ground motion frequency content on the developed hoop strains, wavelet pulses were employed for analysis having an amplitude of 1.0g and a predominant frequency f_g varying from 1.0 Hz to 9.0 Hz. More precisely, Ricker wavelets (Ricker 1943) were used to excite a series of models with varying structural frequency ratio f_B/f_A ranging from 0.30 to 2.73 (corresponding to a variation of f_B ranging from 1.0 Hz to 9.0 Hz while f_A was kept equivalent to 3.3 Hz), representing the pulse-like waveforms of acceleration inputs with a narrow frequency bandwidth (Fig.2).

Inspection of $D_{diff,max}$ (Fig.3, a) and $\epsilon_{h,max}$ (Fig.3, b) results over the variation of structural frequency ratio f_B/f_A reveals non-zero responses in all cases except when $f_B/f_A = 1.0$. For these cases, a minimum $D_{diff,max}$ response of around 25 mm and a minimum $\epsilon_{h,max}$ response of around 0.1% exist even when none of the structure natural frequencies f_A and f_B are close to the predominant frequency of excitation f_g . This indicates that the out-of-phase oscillation between two supporting structures can occur as long as their first-mode natural frequencies of vibration are not identical. On the pipe elbows, hoop strain develops accordingly during the excitation as the elbows bend due to the differential motion exerted between the two pipe-ends.

Inspection of $D_{diff,max}$ and $\epsilon_{h,max}$ results over the variation of input predominant frequency f_g shows the fact that the responses will reach local maximum values when resonance to the input excitation occurs for at least one of the supporting structures. For all models with a f_B/f_A value other than 1.0, wavelet excitation with predominant frequencies $f_g = 3.0$ Hz and $f_g = 3.5$ Hz have led to $D_{diff,max}$ response greater than 58 mm and $\epsilon_{h,max}$ response higher than 0.51%, which can be attributed to the resonance of structure A (whose natural frequency $f_A \equiv 3.3$ Hz) to these inputs. We note that the responses observed in these cases are nearly constant as long as structure A is the only resonant supporting structure. A series of peaks goes diagonal across the 3D plots (i.e. from the point [$f_g = 1.0$ Hz,

252 $f_B/f_A = 0.3]$ to the point [$f_g = 9.0$ Hz, $f_B/f_A = 2.73]$) reflect the resonance of structure B (whose natural frequency
 253 f_B varies between 1.0 Hz to 9.0 Hz) to the corresponding wavelet excitation. These diagonal peaks are higher as the
 254 natural frequency of structure B f_B and the predominant frequency of excitation f_g are lower. Moreover, we notice that
 255 the $D_{diff,max}$ and the $\epsilon_{h,max}$ responses further amplify when the natural frequencies of the two supporting structures,
 256 f_A and f_B , are both close to the predominant frequency of excitation f_g . Within the scheme of this parametric study,
 257 the phenomenon is observed at the analysis case $f_g = 3.0$ Hz and $f_B/f_A = 0.92$ (i.e. $f_A \equiv 3.3$ Hz, $f_B = 3.04$ Hz),
 258 which results in $D_{diff,max} = 120$ mm and $\epsilon_{h,max} = 0.78\%$. Notice that this $D_{diff,max}$ value is almost exactly twice
 259 as much as the $D_{diff,max}$ values observed in cases where structure A is the sole supporting structure in resonance
 260 with the $f_g = 3.0$ Hz wavelet input, whereas the $\epsilon_{h,max}$ value is intensified by around 50%.

261 Looking through all analysis cases, the global maximum values of $D_{diff,max}$ and $\epsilon_{h,max}$ occur at the analysis case
 262 $f_g = 1.0$ Hz and $f_B/f_A = 0.30$ (i.e. $f_A \equiv 3.3$ Hz, $f_B = 1.0$ Hz), resulting in $D_{diff,max} = 274$ mm and $\epsilon_{h,max} = 2.32\%$.
 263 The above observations indicate that a combination of supporting structures with low first-mode natural frequencies
 264 (either a single or both the supporting structures) and ground excitation with a low predominant frequency can lead to
 265 the onset of higher out-of-phase vibrations between the two supporting structures, hence a higher seismic elbow strain
 266 demand.

267 Of course, real earthquake ground motions are typically rich in a broader range of frequency contents. A selection
 268 of five earthquake accelerograms with different predominant frequencies (Table 2 and Fig.4) and their PGA scaled
 269 to $a_g = 1.0$ g were used to excite the FE models with varying f_B/f_A values. Note that the intention of this practice
 270 was not to extensively explore the impact of different ground motions to the proposed structure-pipe-structure scenario
 271 but to provide a proof that the observations gained from the wavelet cases are also conceptually applicable for real
 272 ground motions. While similar trends can be qualitatively confirmed by interpreting Fig.3, c and Fig.3, d, $D_{diff,max}$
 273 and $\epsilon_{h,max}$ values obtained using ground motion inputs carry greater randomness. Overall, a higher magnitude of
 274 responses can be observed due to the much-longer duration of excitation, where global maximum values $D_{diff,max} =$
 275 391 mm and $\epsilon_{h,max} = 5.26\%$ are indicated at the analysis case $f_g = 1.2$ Hz (i.e. Input motion 5), $f_B/f_A = 0.30$
 276 (i.e. $f_A = 3.3$ Hz, $f_B = 1.0$ Hz). The reference case of the parametric study, $f_g = 2.2$ Hz (i.e. Input motion 4) and
 277 $f_B/f_A = 0.70$ (i.e. $f_A = 3.3$ Hz, $f_B = 2.3$ Hz), which is also the case later tested in HS, is marked on the figures where
 278 $D_{diff,max} = 189$ mm and $\epsilon_{h,max} = 3.13\%$ are predicted.

279 **Effect of the Pipe-end Attachment Point Elevation**

280 Given the same NG pipe, the same structural dynamic properties and the same ground motion input, the dynamic
 281 response of the structure-pipe-structure system can be different depending on the specific location, in particular, the
 282 elevation of the attachment points where the two ends of the linking pipe element are connected to the supporting
 283 structures. In the parametric study, the two pipe-end attachment points have identical elevation and their variations are

284 assumed simultaneous so that a single parameter, i.e. pipe-end attachment elevation H_p , is sufficient for describing
285 the phenomenon. A reasonable variation of H_p in the range of 2.0 m to 8.0 m was considered to account for NG
286 pipes connected at different heights between two typical industrial structures in NG plants. Note that because the two
287 supporting structures are represented by equivalent SDOF oscillators, the simplified FE models have the limitation in
288 replicating the true profile of structural lateral deformation along their elevation during the excitation. This means the
289 analysis accuracy reduces when the pipe-end attachment elevation H_p is far off from the elevation of mass centres of
290 the SDOF supporting structures H_s , which is equivalent to 5.3 m. Nevertheless, the impact of varying H_p to the global
291 and local system responses can be reflected.

292 Within the range of examined pipe-end attachment elevation H_p values, analysis result shows an linearly correlated
293 relationship between the H_p and the $D_{diff,max}$ response (Fig.5, a). The $D_{diff,max}$ maxes out at 296 mm and reaches
294 its minimum of 43 mm when the pipe-end attachment elevation is $H_p = 8.0$ m and $H_p = 2.0$ m, respectively. On the
295 other hand, while the $\epsilon_{h,max}$ response (Fig.5, b) also becomes larger as the H_p is larger, the correlation is not linear.
296 Compared to the reference case in which $H_p = 5.3$ m, increasing the H_p value by 2 m intensifies the $\epsilon_{h,max}$ output by
297 no more than 16%, whereas decreasing the H_p value by the same amount results in around 40% of reduction on the
298 $\epsilon_{h,max}$ response.

299 **Effect of the Structural Stiffness**

300 An important property of the coupled structure-pipe-structure system is characterised by the relative ratio between
301 the stiffness of the linking pipe element and those of the supporting structures. Considering the fact that a total of two
302 structures are involved in the scenario with different swaying stiffness values and the nonlinear behaviour expected
303 for the linking pipe element, we herein examine only the variation of the linear elastic equivalent SDOF structural
304 stiffness and use it to conceptualise the variation of pipe-structure stiffness ratio, instead of defining the ratio explicitly.
305 A higher input of structural stiffness indicates a lower pipe-structure stiffness ratio and vice versa. In the parametric
306 study, the stiffness of the two structures, K_A, K_B , are assumed to vary simultaneously so that their values in different
307 analysis cases can be expressed using a single percentage value with regard to the reference model. To give an idea, the
308 linear elastic equivalent SDOF swaying stiffnesses of structure A and structure B in the reference case are $K_A = 52670$
309 kN/m and $K_B = 16670$ kN/m, while the x-axis initial stiffness of the linking pipe element is equivalent to 751.5 kN/m.
310 Additionally, in order to reflect the case when pipe-structure stiffness ratio is zero, we also analysed the aforementioned
311 models with the linking pipe element being removed. Note that the variation of K_A, K_B is always accompanied by
312 a corresponding change of equivalent SDOF masses of the two structures, so that the natural frequencies of the two
313 supporting structures are kept invariant in this section.

314 The $D_{diff,max}$ (Fig.5, c) and $\epsilon_{h,max}$ (Fig.5, d) responses are plotted against structure stiffness K_A, K_B . The
315 $D_{diff,max}$ response is higher for cases when structural stiffness is higher (i.e. lower pipe-structure stiffness ratio),

316 indicating a weakened coupling effect between the two supporting structures introduced by the weaker linking pipe
317 element. Also, we observe constant numerical outputs of $D_{diff,max} = 212$ mm for all analysis cases when the linking
318 pipe element is removed, represented by the dotted line on Fig.5, c. The $D_{diff,max}$ curve continually approaches
319 the dotted line but does not meet it within the range of examined K_A, K_B . One might perceive that the curve and
320 the dotted line will never meet at any finite value of structural stiffness as long as the linking pipe element keeps its
321 presence, hence its stiffness. A similar trend applies to the $\epsilon_{h,max}$ response as well. As the structure-pipe-structure
322 interaction is weakened due to a higher K_A, K_B input, the elbow strain demand correspondingly raises and approaches
323 a theoretical maximum value as the pipe-structure stiffness ratio approaches zero. For the proposed structure-pipe-
324 structure configuration, the $D_{diff,max}$ result exceeds 95% of the no-pipe cases when structural stiffness percentage
325 exceeds 180% of the reference model, in which case $K_A = 105340$ kN/m and $K_B = 33330$ kN/m. In such a case
326 when the pipe-structure stiffness ratio is lower than a certain level hence the $D_{diff,max}$ response does not clearly
327 deviate from the corresponding no-pipe case, a coupled analysis is rendered unnecessary. This means predetermined
328 structural responses from a no-pipe case can be used as inputs to predict seismic demand of the linking pipe element
329 with acceptable accuracy. However, we stress that a coupled analysis is always recommended in the preliminary stage
330 of any pipe-related researches where similar structure-pipe-structure configurations are involved, so that the boundary
331 condition of the pipe can be made sure realistic. Additionally, when deciding whether a coupled analysis can be
332 neglected, it would be a good practice to inspect not only the peak value $D_{diff,max}$ but the quantity's full time
333 variation $D_{diff}(t)$ when possible.

334 **Effect of the Straight Pipe Length Between Two Elbows and the Perpendicular Distance Between Two Supporting** 335 **Structures**

336 The length of the straight pipe segment between the two 90-degree elbows L_z and the perpendicular distance
337 between the two supporting structures L_x are variables describing the different geometry layouts of the linking pipe
338 element. The examined range of L_z was selected as 1.0 m to 3.0 m and the range of L_x was selected as 4.0 m to 9.0
339 m. Within these ranges the overall length and shape of the linking pipe element is realistic for typical bridging pipes
340 within NG plants while further complicating the parametric study by adding a pipe rack is avoided. The two 90-degree
341 elbows are assumed to always locate exactly at the middle, forming the linking pipe element a symmetrical shape.

342 The $D_{diff,max}$ response are found to have a very weak dependency on the variation of L_z (Fig.5, e) as the deviation
343 of responses between all cases are less than 10%. On the other hand, the $\epsilon_{h,max}$ response reduces significantly as the
344 L_z is larger (Fig.5, f), there is a 50% reduction on elbow strain demand as the L_z increases from the reference case of
345 to 3.0 m. The similar global displacement responses of the structures with respect to different L_z inputs is because the
346 x-axis stiffness of the linking pipe element remains almost unchanged within the range of L_z variation. Meanwhile, a
347 shortened L_z means that the elbows are subjected to a larger bending angle, hence a much higher local elbow strain

348 demand. On the other hand, the variation of L_x has led to almost constant $D_{diff,max}$ (Fig.5, g) and $\epsilon_{h,max}$ (Fig.5, h)
349 responses, where the deviation between all cases is less than 3% and 10%, respectively.

350 **Effect of Pipe Internal Pressure**

351 NG is usually highly compressed for its transmission through pipes. In the parametric study, pipe internal pressure
352 P in the range from zero to 80% of the reference pipe's nominal yield stress, $80\%p_y = 80\%(2\sigma_{y,1t}/D) \approx 12.5$ MPa,
353 was examined. Note that the uniqueness of variable P from the rest of the variables examined in the parametric study
354 is that the internal pressure affects both the demand and the capacity of the pipe. The collapse moment of pipe elbows
355 is known to increase with higher internal pressure up to a certain threshold value, and then decrease with further
356 increasing of internal pressure. Previous research showed that for the 90-degree elbows with bend factor $h \approx 0.16$,
357 this threshold value is around $P = 10.5$ MPa when the elbows are subjected to closing bending moment (Shalaby and
358 Younan 1998).

359 The peak differential displacement between two pipe-ends $D_{diff,max}$ is lower as a result of higher P input (Fig.5,
360 i). This is because an increased pipe internal pressure can lead to higher x-axis stiffness of the linking pipe element,
361 hence a more pronounced structure-pipe-structure interaction to mitigate the differential displacements between two
362 supporting structures. However, although the $D_{diff,max}$ response tends to reduce with higher P so that effectively
363 the 90-degree elbows are less bent during the excitation, its benefit to the alleviation of seismic elbow strain demand
364 is completely suppressed by the presence of the higher pipe internal pressure itself. The maximum elbow hoop strain
365 $\epsilon_{h,max}$ soars as the P input increases (Fig.5, j).

366 **EXPERIMENTAL SET-UP: HYBRID SIMULATION**

367 **System Substructuring Scheme**

368 Considering the non-negligible structure-pipe-structure interaction and the size of the interactive industrial struc-
369 tures, HS is believed a necessary and efficient way for experimentally investigating the buckling potential and the
370 detailed nonlinear hysteretic behaviour of the linking pipe element as well as the interactive response of the overall
371 system. We developed an HS scheme based on the reference model used in the parametric study, in which a physical
372 specimen of the linking pipe element, consisting three straight pipe segments and two 90-degree elbows, was tested
373 at the Structures Laboratory of the University of Patras, Greece whereas the complementary part involving the two
374 supporting structures was solved numerically (Park et al. 2021). A total of two substructure modules, as illustrated in
375 Fig.6 and will be discussed in the following sections, were therefore configured for the HS in order to investigate the
376 coupled response of the structure-pipe-structure system.

377 The generalised HS framework, UT-SIM, developed by the University of Toronto research group (Huang and Kwon
378 2018; Mortazavi et al. 2017) was used for integrating the numerical and experimental substructures. The UT-SIM
379 framework employs the University of Toronto Networking Protocol (UTNP) for communication while a software library

380 provides useful functions in exchanging data between diverse numerical and experimental models. The generalised
381 nature of UT-SIM framework assigns each substructure module with an interface of communication. In this HS
382 scheme, OpenSees computational platform (Mazzoni et al. 2006) was selected to perform the analysis tasks of solving
383 both the numerical substructure and the main integration algorithm. Therefore, an OpenSees user defined element
384 termed *SubStructure* was featured to the numerical model to collect the required restoring force through UTNP. On the
385 other hand, a software called the network interface for the controller (NICON) (Zhan and Kwon 2015), based on the
386 *LabView* programming environment and *National Instrument* hardware, allows communication, coordinate conversion,
387 analogue voltage generation, data transmission and acquisition of the physical substructure module.

388 During the entire HS, the numerical integration algorithm calculates a set of command displacements (u_A, u_B)
389 at each analysis time step. This digital information is passed from the numerical integration module to the physical
390 substructure module via the UTNP-utilising communication interfaces featured in the UT-SIM framework, consisting
391 of the *SubStructure* OpenSees element for the former and the NICON software for the latter. The calculated structural
392 displacements are received by the NICON and go through a simple calculation which turns them into the differential
393 displacement to be imposed to the physical pipe specimen ($D_{diff}(t) = u_A(t) - u_B(t)$), before the command is then
394 converted into an analogue voltage signal employing *National Instrument* data acquisition digital-to-analog conversion
395 hardware. The generated displacement command is subsequently interpreted by a modular actuator controller unit,
396 which drives the unidirectional hydraulic actuator using proportional–integral–derivative (PID) control. Given an
397 accurate actuation control and the fact that strain rate effect due to seismic motion is believed to have little influence
398 on the material stress-strain behaviour of pipe (Yoshizaki et al. 2000), the overall structure-pipe-structure system
399 is subjected to deformations and damage equal to those a real earthquake would generate. The structural response
400 parameters (actuator force and actually imposed displacement) are not known in advance and are measured and recorded
401 during the HS via the actuator load cell and a high-resolution Temposonics transducer attached on the actuator. The
402 restoring force and displacement responses of the physical substructure acquired at the current time step, are converted
403 to digital form and fed back to the numerical integration algorithm. Eventually the current time step is completed and
404 HS progresses to the next one until full completion of the excitation record.

405 **Numerical Integration Module**

406 The numerical integration module of the proposed HS scheme contains the FE model representing the two supporting
407 structures in the proposed structure-pipe-structure scenario and handles the main integration algorithm for dynamic
408 time history analysis. The linear elastic equivalent SDOF modelling approach used in the parametric study for the
409 two supporting structures was transplant to the HS in the OpenSees numerical integration module. By employing the
410 modelling approach and applying the identical assumptions and boundary conditions to the numerical substructure,
411 we ensure the compatibility and equilibrium condition at the numerical-physical coupling DOF (i.e. x-axis differential

412 motion between the two pipe-ends) so that a single unidirectional actuator is sufficient for applying the appropriate
413 boundary condition to the physical substructure module during HS. Note that in the OpenSees model, the equivalent
414 SDOF columns were modelled using the Elastic Timoshenko Beam-Column Element, which employs the same beam
415 theory as the ABAQUS B31 element used in the parametric study models. A dedicated *SubStructure* element was
416 defined, acting as the interface of communication for the numerical substructure. Furthermore, supporting structure
417 properties employed in the numerical integration module were identical to those of the reference case in the parametric
418 study. Structure A had a natural frequency of $f_A = 3.3$ Hz and mass of $M_A = 122.5$ tonne; structure B had a natural
419 frequency of $f_B = 2.3$ Hz and mass of $M_B = 79.8$ tonne. The numerical model was assigned with 2% Rayleigh
420 damping and Alpha - Operator Splitting method (Combescure and Pegon 1997) was used as the integration algorithm.
421 The total analysis period of the HS was set to 10 s, corresponding to a total of 1,000 time steps as the step size was
422 selected to be 0.01 s. The first 7 s of the accelerogram from the 1972 Nicaragua Earthquake recorded at the Managua
423 ESSO station (i.e. input motion 4 as shown in Fig.4), with a predominant frequency of 2.2 Hz and the PGA scaled to
424 1.0 g, was used as the input ground motion to the numerical integration module in HS.

425 The effectiveness of the numerical integration module was verified by a series of OpenSees-ABAQUS multi-
426 platform simulations prior to the actual HS, where the physical substructure module containing the linking pipe
427 specimen was represented by an ABAQUS numerical replacement. Accuracy and stability of the integration process,
428 effectiveness of the OpenSees numerical model and the smooth operation of the associated UT-SIM framework
429 components which cooperate with the numerical substructure were double-checked.

430 **Physical Substructure Module**

431 The physical substructure module is composed of the full-scale physical specimen of the linking NG pipe and
432 relevant accessories including a hydraulic actuator, an actuator controller, the HS interface software NICON which
433 links the actuator controller to the numerical model, the measuring instruments and a data acquisition system.

434 The physical NG pipe specimen residing at the Structures Laboratory of the University of Patras, Greece (Fig.6),
435 includes three straight pipe segments welded in-situ on two 90-degree elbows with a cross-sectional diameter (D)
436 of 219.6 mm and a pipe wall-thickness (t) of 6.3 mm. The length of the straight pipe segment located between the
437 two elbows (L_z) is 1.38 m, the length of the other two straight pipe segments is 3.48 m and the bend radius of the
438 90-degree elbows (R) equals 302.0 mm. Therefore, the perpendicular distance between the two structures (L_x) is
439 7.56 m, the pipe nondimensional geometry parameters are $R/D = 1.38$, $D/t = 34.86$ and the elbow bend factor is
440 $h = Rt/(D/2)^2 = 0.16$. Before the HS, a water pumping system applied pipe internal pressure (P) of 3.0 MPa to the
441 pipe specimen, accounting for the compressed NG inside the pipe. In the laboratory, the pipe specimen was rigidly
442 clamped onto the strong laboratory floor through a triangular connector at one end, while its other end was attached to
443 an unidirectional actuator. A low-friction guiding device was set up around the straight pipe segment near the actuator

444 side, limiting the actuator's movement along the x-axis. This was to ensure the SDOF equilibrium condition at the
445 numerical-physical coupling node so that the errors introduced at the interface between two HS substructures were
446 minimised. On the other hand, because the pipe specimen was in contact with the guiding device, a contact force
447 with unknown magnitude was inevitably included as part of the specimen restoring force since potential horizontal
448 or vertical pipe inclination might occur during the HS. As a result, a small error may still exist in the force feedback
449 to the numerical integration module at every analysis time step, which could harm the accuracy of HS result. While
450 all contacting surfaces between the pipe and the guiding device were covered with Teflon sheets and were highly
451 lubricated to reduce friction, the upper-half of the guiding device was also left rather loose to further reduce the impact
452 of contact/pipe inclination to its minimum. Two strip supports with Teflon and lubricated flat surfaces were placed
453 under the middle of the pipe specimen to provide pipe constraint in the vertically downward direction, simulating the
454 single-column pipe support in the proposed structure-pipe-structure configuration. By doing so, initial pipe flexure
455 due to its self-weight was prevented.

456 The effectiveness of the laboratory set-up was validated to ensure the presence of the auxiliary gears do not obstruct
457 the validity of our model assumptions. Evidences obtained during and after preliminary non-damaging HS showed
458 a minor effect of the contacting force originated from the restraint device and the strip supports. We noted that the
459 pipe specimen started to deform elastically at a very small applied actuator displacement, indicating a very small
460 unwanted contacting force in the laboratory set-up. The force is experimentally estimated at less than 2% of the
461 maximum restoring force that the linking pipe specimen would experience during the full-amplitude HS. Given the
462 above discussion, it is concluded that experimental results obtained from the HS laboratory set-up are valid.

463 Still, if not tuned properly, the HS set-up can generate erroneous results for various other reasons. These may
464 include the working frequencies and amplitudes of the physical set-up, the condition of the tested specimen, the
465 actuator, the control device, the type of the chosen control algorithm and its parameter setting, as well as the selected
466 size of the ramp and hold periods for each analysis time step (Molina et al. 2011). Hence, the effectiveness of the
467 physical substructure module was further optimised and verified by a series of nondestructive HS prior to the actual
468 HS. Firstly, through trial and error, appropriate parameters of the PID controller as well as the allowable velocity of
469 the actuator were determined so as to confront the noise in the reference (analog) signal due to A/D conversion and
470 to minimize control error. By the same token, low actuator responsiveness yields the need for longer stabilization
471 period at the end of the ramp and an appreciable hold period for averaging an adequate number of restoring force
472 sample values (analog). As a result, testing wall-clock time increased considerably. In the trade-off between HS
473 accuracy and time-efficiency, an appropriate maximum actuator speed was selected equal to 1 mm/s, and a waiting
474 period of 5 s was used after each execution of command displacement so as to reduce the undesirable fluctuation of
475 forces. An averaged measurement of reaction force was designed to be taken in a period of 2 s after the 5 s-waiting, so
476 that the noise-to-signal ratio in the measurement can be further reduced. Such a configuration ensures the numerical

477 integration module to get representative force and displacement feedback from the physical substructure module, while
478 producing a relatively reasonable 6-hour HS execution time. Moreover, the initial stiffness of the physical NG pipe
479 specimen, which is required as an input variable for the Alpha - Operator Splitting numerical integration algorithm,
480 was experimentally measured.

481 **Instrumentation**

482 *Strain Gauges*

483 A 16-channel data acquisition system for strain measurement was used for the test. The strain gauges were installed
484 as shown in Fig.7, a. The four locations with significant strains on an half-elbow were identified based on numerical
485 analyses. Because of the possible out-of-plane deformation of the pipe and the existence of the restraint device, the pipe
486 specimen may behave unsymmetrically despite its symmetrical geometry. Thus, all four half-elbows were instrumented
487 with strain gauges at the same locations to ensure the measurement of maximum strains on the elbows.

488 *Ovalization measuring devices*

489 Two special-purpose ovalization measuring devices (one per elbow) with LVDTs were used in order to measure the
490 development of cross-sectional ovalization on the elbows (Fig.7, b). The main body of the ovalization measurement
491 device is a light steel frame which is in contact with the elbow at four points along the perimeter of a single cross-section:
492 the frame is welded to the elbow at its intrados, whilst displacement measurements are taken at the elbow's extrados
493 and two flanks. The steel frame itself is considered rigid, allowing the LVDTs to be pressed against the elbow wall,
494 thus obtaining the correct measurement of elbow cross-sectional diameter change, or "flattening" (Varelis et al. 2012),
495 at two perpendicular pipe diameters. The devices are installed in the middle (45-degree) section of the elbows, where
496 maximum elbow flattening was predicted. Preliminary numerical analysis also proofed a negligible impact to the pipe
497 responses brought by the welded ovalization devices.

498 **OBSERVATIONS AND RESULTS FROM HYBRID SIMULATION**

499 The examined linking NG pipe element showed a favourable performance under the specific structure-pipe-structure
500 configuration and the input earthquake ground motion during which no leakage was observed. The HS confirmed the
501 minor influence of the contacting force originated from the auxiliary restraint device and the strip supports, and no
502 out-of-plane deformation of the pipe specimen was observed during the HS.

503 **Differential Displacement Time History and Force-Displacement Relationship**

504 Time history of differential displacement between the two pipe-ends, $D_{diff}(t)$, and force-displacement relationship
505 of the linking NG pipe (Fig.8) obtained from the HS (*HS holistic*) and its corresponding numerical model in ABAQUS
506 (*FEA holistic*) are compared to gain insight into the hysteretic response of the linking pipeline element. The $D_{diff}(t)$
507 response represents the system response on a global level, whereas the force-displacement curve reveals evident

508 hysteresis behaviour of the pipe. The $D_{diff}(t)$ response of the HS is very similar to its finite element analysis (FEA)
509 counterpart in the first-half of the ground motion, leading to identical peak differential displacement between two
510 pipe-ends at $D_{diff,max} = 189$ mm. As the input excitation gradually dies down, more discrepancy between the two
511 curves are observed. It is also noted that while the FEA holistic model of the structure-pipe-structure system predicted
512 well the amplitude of relative displacement time history, the result obtained from HS showed a slightly higher vibration
513 frequency. Additionally, the $D_{diff}(t)$ response of standalone structures without being coupled by the linking pipe
514 element (*FEA no pipe*) is presented showing the impact of structure-pipe-structure interaction.

515 **Strains on Elbows**

516 Four groups of strains were monitored at the top and bottom surfaces of the two elbows to account for the possible
517 unsymmetrical behaviour of the pipe specimen during the HS due to the presence of the constraint device. Despite
518 this concern, test results were found similar on the two elbows. Critical hoop strain measurement from the HS, $\epsilon_h(t)$,
519 sampled physically at the locations corresponding to where the maximum elbow hoop strain was observed in numerical
520 predictions, is plotted in Fig.9. We note that measurement on the bottom side of Elbow 1 shows zero strain and the
521 measurement on the top side of Elbow 2 saturates after 5 s into the HS. These errors can be attributed to a detached
522 or a damaged gauge. Ratcheting effect of strain development is clear from both HS results and FE prediction. The
523 maximum elbow hoop strain during the HS occurred on the top side of Elbow 1 (i.e. the one close to the actuator)
524 at $\epsilon_{h,max} = 3.49\%$, whereas the FE predicts $\epsilon_{h,max} = 3.13\%$. Moreover, the ratchet effect of elbow hoop strain
525 development recorded during the HS was only approximately captured by FEA, in which the time spot when $\epsilon_{h,max}$
526 occurs and the general trend of strain development was quite different.

527 **Cross-sectional Ovalization**

528 Cross-sectional ovalization is quantified and visualised in the form of cross-sectional flattening, i.e. the change of
529 elbow diameter in a certain direction (Fig.10, a). The horizontal and vertical cross-sectional flattening on both elbows
530 were compared against the numerical prediction. The hybrid simulation result shows a less significant permanent
531 cross-sectional flattening at the vertical direction when compared to the numerical prediction: at around 2.5 s to 3.5 s
532 on the time history, the centre line of the *FEA-vertical* curve shifted upward with a magnitude of about 5 mm, while
533 maintaining a similar level of vibration compared to the HS result. The same trend was also observed through an
534 inspection of the corresponding flattening- D_{diff} curve in Fig.10, b. Because the ovalization results are similar on
535 both elbows, only those from one of the elbow are shown.

536 **CONCLUDING REMARKS**

537 In this paper, the seismic performance of a coupled structure-pipe-structure system typically found in an NG
538 processing plant was assessed by means of hybrid simulation (HS). A parametric study was firstly performed based on
539 simplified FE models and the HS was conducted in which the holistic system was simulated as two coupled substructures

540 so the linking NG pipe can be modelled physically in full-scale. Reliable boundary conditions of the linking NG pipe
541 were established in our investigation by modelling explicitly the two supporting structures and analysing the coupled
542 structure-pipe-structure system as a holistic integer. Although the x-axis stiffness of the linking pipe element is much
543 smaller than the swaying stiffness of the supporting structures, simulation results show a clear coupling effect introduced
544 by its presence. Globally, differential displacement between the two supporting structures reduces up to 40% through
545 the duration of the ground excitation for the reference analysis case due to the presence of the linking pipe element,
546 indicating that the structure-pipe-structure interaction should not be overlooked for the proposed scenario and an HS is
547 necessary for capturing the interaction experimentally. Locally, the connection of the linking pipe element to a total of
548 two supporting structures with distinguishing dynamic properties contributes to the differential displacement between
549 two pipe-ends, hence the pronounced out-of-phase oscillation. As a result, the two pipe elbows can be bent severely
550 into their nonlinear range.

551 The triggering factors of critical seismic demand for the linking NG pipe in the proposed structure-pipe-structure
552 scenario are summarised as follows:

- 553 • The simultaneous mobilisation of divergent structural oscillation at the low-frequency range between the two
554 supporting structures: It leads to high responses both globally and locally, which can be attributed to the adverse
555 combination of variable f_B/f_A , f_g and H_p , i.e. natural frequency ratio of the supporting structures, predominant
556 frequency of excitation and the elevation of pipe-end attachment points. Peak differential displacement between
557 two pipe-ends, $D_{diff,max}$, and maximum local elbow hoop strain, $\epsilon_{h,max}$, are at their highest when the two
558 supporting structures have different natural frequencies both in the low-frequency range and are both resonant
559 to the input ground motion. Meanwhile, the elevation of pipe connecting points directly affects how much the
560 linking pipe element can be exposed to the generated differential displacements between the two supporting
561 structures, given the same input earthquake, the same structures and the same pipe properties.
- 562 • A lower relative stiffness of the linking pipe element with respect to that of the structures: In general, a lower
563 pipe-structure stiffness ratio leads to a lower structure-pipe-structure interaction, hence higher $D_{diff,max}$ and
564 $\epsilon_{h,max}$ responses.
- 565 • Adverse geometry characteristic of linking pipe element: As the length of the straight pipe segments varies,
566 the stiffness of the linking pipe element is barely affected. However, given the similar $D_{diff,max}$ responses,
567 a linking pipe element with shorter straight pipe segments means that the two 90-degree elbows are more
568 susceptible to bending, hence a higher seismic elbow strain demand.
- 569 • A higher pipe internal pressure P : The existence of pipe internal pressure naturally introduce a static load on
570 pipe hence increases the elbow strain demand. Its potential benefit in mitigating excessive $D_{diff,max}$ response,
571 thanks to the simultaneous pipe stiffness increase, is completely overshadowed by the increased pressure load

572 itself.

573 Adjusting these variables to the unfavourable side can lead to significantly increased seismic demand to the pipe elbows.
574 It is particularly true for the variables f_B/f_A and f_g , H_p , as well as P . Even when configuring only one of these
575 variables from the reference scenario, which is a typical industrial site and is therefore deemed as a ‘probable scenario’,
576 to a ‘worst-case scenario’, where maximum responses were observed from the parametric study, can easily result in at
577 least an 30% increase of the elbow strain demand.

578 Compared well with the corresponding FE predictions, HS results show a peak differential displacement response
579 between the two pipe-ends of 189 mm and a maximum elbow hoop strain of 3.49% for the reference model. Pipe
580 yielding, material plasticity and strain ratcheting were observed on the elbows together with a clear asymmetric
581 hysteretic behaviour of the linking pipe element, which is mainly due to the nonlinear geometry of the linking pipe
582 element and the ovalization of pipe cross-section. On the other hand, pipe buckling or a loss of containment event did
583 not occur under this level of elbow strain demand generated during the 7 s-earthquake excitation of the HS.

584 Overall, the present study shows that the structure-pipe-structure interaction should not be overlooked, and we
585 recommend a coupled analysis to be considered at least in the preliminary stage of future pipe-related studies where
586 similar structure-pipe-structure configurations are involved in a time history analysis, so that the imposed displacements
587 at the boundary of the pipe segment are considered appropriately.

588 **Limitations of the Study and Possible Future Works**

589 The presented study provides a comprehensive evaluation to the seismic demand of coupled NG pipe located
590 within the proposed structure-pipe-structure scenario, which is then verified experimentally through an HS. Although
591 the numerical observations and the HS results were satisfactory, the study has some limitations and thus future works
592 can be devoted to the following four directions. Firstly, due to limited laboratory resources, the authors were only able
593 to execute a single HS, which corresponds to the reference case of the parametric study. The limited stroke of the
594 available hydraulic actuator also meant that an HS for any analysis case with a potentially higher dynamic structural
595 response was not possible. Secondly, the presented numerical and experimental studies did not account for structural
596 nonlinearity, soil-structure interaction as well as a sophisticated modelling of pipe-end connection. Also, only a basic
597 constitutive model was employed in the FE analyses to simulate the cyclic nonlinearity of the pipe steel material.
598 Efforts can be put into those directions in the future, making use of refined FE models, to examine in a greater detail
599 the proposed structure-pipe-structure scenario. Thirdly, investigations involving an extensive collection of earthquake
600 ground motions can be made to derive fragility curves for the proposed scenario and gain deeper insight to the dynamic
601 nature of the system in a probabilistic manner. Finally, given that the strain development on a steel pipe elbow is
602 cumulative with regard to the total number of excitation cycles it undergoes, future works can be done to account for
603 the effect of multiple earthquake events on the seismic elbow strain demand and its possible damage modes. This will

604 address the potential seismic threat to steel NG pipe elbows in which they fail because of low cycle fatigue during their
605 entire service life-span after experiencing a number of strong ground motions, despite immediate loss of pipe integrity
606 in terms of buckling failure may not appear during a single earthquake event.

607 **DATA AVAILABILITY STATEMENT**

608 Some or all data, models, or code that support the findings of this study are available from the corresponding author
609 upon reasonable request. Items included are the ABAQUS finite-element models and scripts used in the parametric
610 study, the numerical data from the parametric study, the OpenSees finite-element model used in the hybrid simulation,
611 files and software associated to the UT-SIM framework used in the hybrid simulation and the experimental data from
612 the hybrid simulation.

613 **ACKNOWLEDGEMENTS**

614 This work was funded by the Horizon 2020 Programme of the European Commission through grant MSCA-
615 RISE-2015-691213-EXCHANGE-Risk (Experimental & Computational Hybrid Assessment of Natural Gas Pipelines
616 Exposed to Seismic Risk, www.exchange-risk.eu). The first author also expresses his gratitude to the China Scholarship
617 Council for financially supporting his doctoral studies (Grant No.: 201808060061).

618 **REFERENCES**

- 619 Bursi, O. S., di Filippo, R., La Salandra, V., Pedot, M., and Reza, M. S. (2018). “Probabilistic seismic analysis of an
620 LNG subplant.” *Journal of Loss Prevention in the Process Industries*, 53, 45–60.
- 621 CEN (2006). *Eurocode 8 - Design of structures for earthquake resistance - Part 4: Silos, tanks and pipelines Eurocode*.
622 EN 1998-4:2006.
- 623 Combescure, D. and Pegon, P. (1997). “ α -Operator splitting time integration technique for pseudodynamic testing
624 error propagation analysis.” *Soil Dynamics and Earthquake Engineering*, 16(7-8), 427–443.
- 625 Dassault Systèmes Simulia Corp. (2014). *Abaqus 6.14 Documentation*. Providence, RI, USA.
- 626 Firoozabad, E. S., Jeon, B.-G., Choi, H.-S., and Kim, N.-S. (2015). “Seismic fragility analysis of seismically isolated
627 nuclear power plants piping system.” *Nuclear Engineering and Design*, 284(1), 264–279.
- 628 Fouquiau, P.-V., Barbier, F., and Chatzigogos, C. (2018). “New Dynamic Decoupling Criteria for Secondary Systems.”
629 *16th European Conference on Earthquake Engineering*, Thessaloniki, Greece.
- 630 GIE (2015). *Gas Infrastructure Europe Security Risk Assessment Methodology*. Brussels, Belgium.
- 631 GIE (2019). *Gas Infrastructure Europe LNG Map 2019*. Brussels, Belgium.
- 632 Guarracino, F., Walker, A., and Giordano, A. (2009). “Effects of boundary conditions on testing of pipes and finite
633 element modelling.” *International Journal of Pressure Vessels and Piping*, 86(2-3), 196–206.
- 634 Gupta, A. K. and Tembulkar, J. M. (1984). “Dynamic decoupling of secondary systems.” *Nuclear Engineering and*
635 *Design*, 81(3), 359–373.

636 Hasegawa, K., Miyazaki, K., and Nakamura, I. (2008). "Failure Mode and Failure Strengths for Wall Thinning Straight
637 Pipes and Elbows Subjected to Seismic Loading." *Journal of Pressure Vessel Technology*, 130(1).

638 Hassan, T., Rahman, M., and Bari, S. (2015). "Low-Cycle Fatigue and Ratcheting Responses of Elbow Piping
639 Components." *Journal of Pressure Vessel Technology*, 137(3).

640 Huang, X. and Kwon, O.-S. (2018). "A Generalized Numerical/Experimental Distributed Simulation Framework."
641 *Journal of Earthquake Engineering*, 1–22.

642 Jeon, B.-G., Kim, S.-W., Choi, H.-S., Park, D.-U., and Kim, N.-S. (2017). "A Failure Estimation Method of Steel Pipe
643 Elbows under In-plane Cyclic Loading." *Nuclear Engineering and Technology*, 49(1), 245–253.

644 Karamanos, S. A. (2016). "Mechanical Behavior of Steel Pipe Bends: An Overview." *Journal of Pressure Vessel
645 Technology*, 138(4).

646 Karvelas, C., Stathas, N., Strepelias, E., Palios, X., Chatzopoulou, G., Bousias, S., and Karamanos, S. (2019). "Strong
647 Cyclic Loading of an Industrial Piping System." *2nd International Conference on Natural Hazards & Infrastructure*,
648 Chania, Greece.

649 Lanzano, G., Santucci de Magistris, F., Fabbrocino, G., and Salzano, E. (2015). "Seismic damage to pipelines in the
650 framework of Na-Tech risk assessment." *Journal of Loss Prevention in the Process Industries*, 33, 159–172.

651 Mazzoni, S., McKenna, F., Scott, M. H., and Fenves, G. L. (2006). *Open System for Earthquake Engineering Simulation
652 (OpenSees) - OpenSees Command Language Manual*.

653 Molina, F. J., Magonette, G., Pegon, P., and Zapico, B. (2011). "Monitoring Damping in Pseudo-Dynamic Tests."
654 *Journal of Earthquake Engineering*, 15(6), 877–900.

655 Mortazavi, P., Huang, X., Kwon, O.-S., and Christopoulos, C. (2017). *Example manual for University of Toronto
656 Simulation (UT-SIM) Framework. An open-source framework for integrated multi-platform simulations for structural
657 resilience (Second edition)*. Technical Report, International Workshop on Hybrid Simulation, Department of Civil
658 Engineering, University of Toronto, Canada.

659 Nakamura, I. and Kasahara, N. (2016). "Trial Model Tests With Simulation Material To Obtain Failure." *Proceedings
660 of the ASME 2016 Pressure Vessels and Piping Conference*, Vancouver, British Columbia, Canada, 1–11.

661 Nakamura, I. and Kasahara, N. (2017). "Excitation Tests on Elbow Pipe Specimens to Investigate Failure Behavior
662 Under Excessive Seismic Loads." *Journal of Pressure Vessel Technology*, 139(6).

663 Nakashima, M., Lavan, O., Kurata, M., and Luo, Y. (2014). "Earthquake engineering research needs in light of lessons
664 learned from the 2011 Tohoku earthquake." *Earthquake Engineering and Engineering Vibration*, 13(1), 141–149.

665 Park, J., Zhang, Z., Kwon, O., Bousias, S., and Sextos, A. (2021). "Hybrid Testing for Assessing the Coupled Seismic
666 Response of a Natural Gas Pipeline Linking Two Structures Within a Pressurising Station." *17th World Conference
667 on Earthquake Engineering*, Sendai, Japan.

668 Psyrras, N., Kwon, O., Gerasimidis, S., and Sextos, A. (2019). "Can a buried gas pipeline experience local buckling

during earthquake ground shaking?." *Soil Dynamics and Earthquake Engineering*, 116, 511–529.

669
670 Psyrras, N., Sextos, A., Crewe, A., Dietz, M., and Mylonakis, G. (2020). "Physical Modeling of the Seismic Response
671 of Gas Pipelines in Laterally Inhomogeneous Soil." *Journal of Geotechnical and Geoenvironmental Engineering*,
672 146(5), 04020031.

673 Reza, M. S., Bursi, O. S., Abbiati, G., and Bonelli, A. (2013). "Pseudo-Dynamic Heterogeneous Testing With Dynamic
674 Substructuring of a Piping System Under Earthquake Loading." *Proceedings of the ASME 2013 Pressure Vessels
675 and Piping Conference*, Vol. 8, Paris, France, American Society of Mechanical Engineers.

676 Ricker, N. (1943). "Further developments in the wavelet theory of seismogram structure." *Bulletin of the Seismological
677 Society of America*, 33, 197–228.

678 Sakai, M., Matsuura, S., and Inada, F. (2013). "Hybrid Seismic Response Evaluation Method for Wall Thinning Piping
679 System." *Proceedings of the 2013 21st International Conference on Nuclear Engineering*, Vol. 1, Chengdu, China,
680 American Society of Mechanical Engineers.

681 Sextos, A., Bousias, S., Kwon, O.-S., Di Sarno, L., Kaynia, A., Manolis, G., Crewe, A., Furtner, P., Wenzel,
682 H., Iervolino, I., Baltzopoulos, G., Wuttke, F., Koenke, C., Zabel, V., Borsytsky, R., and Deodatis, G. (2018).
683 "Exchange-Risk : Experimental & Computational Hybrid Assessment of Natural Gas Pipelines Exposed To Seismic
684 Risk." *16th European Conference on Earthquake Engineering*, Thessaloniki, Greece, 1–12.

685 Sextos, A., Manolis, G., Ioannidis, N., and Athanasiou, A. (2017). "Seismically induced uplift effects on nuclear power
686 plants. Part 2: Demand on internal equipment." *Nuclear Engineering and Design*, 318, 288–296.

687 Shalaby, M. A. and Younan, M. Y. A. (1998). "Limit Loads for Pipe Elbows With Internal Pressure Under In-Plane
688 Closing Bending Moments." *Journal of Pressure Vessel Technology*, 120(1), 35–42.

689 Taghavi, S. and Miranda, E. (2008). "Effect of Interaction Between Primary and Secondary Systems on Floor Response
690 Spectra." *The 14th World Conference on Earthquake Engineering*, Beijing, China.

691 U.S. Department of Energy (2017). *Understanding Natural Gas and LNG Options*.

692 Varelis, G. E., Karamanos, S. A., and Gresnigt, A. M. (2012). "Pipe Elbows Under Strong Cyclic Loading." *Volume 8:
693 Seismic Engineering*, Vol. 8, Toronto, Ontario, Canada, American Society of Mechanical Engineers, 45–54.

694 Varelis, G. E., Pappa, P., and Karamanos, S. A. (2011). "Finite Element Analysis of Industrial Steel Elbows Under
695 Strong Cyclic Loading." *ASME 2011 Pressure Vessels and Piping Conference*, Vol. 8, Department of Mechanical
696 Engineering, University of Thessaly, Volos, Greece, ASME, 109–119.

697 Vathi, M., Karamanos, S. A., Kapogiannis, I. A., and Spiliopoulos, K. V. (2017). "Performance Criteria for Liquid
698 Storage Tanks and Piping Systems Subjected to Seismic Loading." *Journal of Pressure Vessel Technology*, 139(5).

699 Vazouras, P., Karamanos, S. A., and Dakoulas, P. (2010). "Finite element analysis of buried steel pipelines under
700 strike-slip fault displacements." *Soil Dynamics and Earthquake Engineering*, 30(11), 1361–1376.

701 Watakabe, T., Nakamura, I., Otani, A., Morishita, M., Shibutani, T., and Shiratori, M. (2017). "Seismic Qualification

702 of Piping Systems by Detailed Inelastic Response Analysis: Part 4 — Second Round Benchmark Analyses With
703 Stainless Steel Piping Component Test.” *Proceedings of the ASME 2017 Pressure Vessels and Piping Conference*,
704 Vol. 8, Waikoloa, Hawaii, USA, American Society of Mechanical Engineers.

705 Wenzel, M., Basone, F., and Bursi, O. S. (2018). “Novel Metamaterial-Based Foundation Concept Applied to a Coupled
706 Tank-Pipeline System.” *Proceedings of the ASME 2018 Pressure Vessels and Piping Conference*, Vol. 5, Prague,
707 Czech Republic, American Society of Mechanical Engineers, 1–12.

708 Yoshizaki, K., Hamada, M., and O’Rourke, T. (2000). “Large deformation behavior of low-angle pipeline elbows
709 subjected to in-plane bending.” *12th World conference on earthquake engineering, paper*, Vol. 1508.

710 Zhan, H. and Kwon, O.-S. (2015). “Actuator controller interface program for pseudo- dynamic hybrid simulation.”
711 *2015 World Congress on Advances in Structural Engineering and Mechanics*, Incheon, Korea, 1–13.

712 **List of Tables**

713 1 List of variables examined in the parametric study 25

714 2 List of earthquake records used as input ground motions 26

TABLE 1. List of variables examined in the parametric study

Symbol	Parameter description	Range of variation
f_B/f_A	The ratio of the natural frequencies of supporting structure B and A	0.30 to 2.73 ($f_A \equiv 3.3$ Hz, $f_B = 1.0$ Hz to 9.0 Hz)
f_g	Predominant frequency of the input ground excitation	1.0 Hz to 9.0 Hz
H_p	Elevation of pipe-end attachment points on the structures	2.0 m to 8.0 m
K_A, K_B	Linear elastic equivalent SDOF swaying stiffnesses of the two supporting structures	50% to 190% of the reference case. At 100%: $K_A = 52670$ kN/m, $K_B = 16670$ kN/m
L_z	Length of pipe between the two 90-degree elbows (Fig.1)	1.5 m to 3.0 m
L_x	Perpendicular distance between two structures (Fig.1)	4.0 m to 9.0 m
P	Pipe internal pressure	0 to 12.5 MPa
D (constant)	Pipe cross-sectional diameter	219.6 mm
t (constant)	Pipe wall-thickness	6.3 mm
R (constant)	Bend radius of the 90-degree elbows	302.0 mm
ρ (constant)	Pipe material density	7.85 tonne/m ³
E (constant)	Pipe material elastic modulus	2.10×10^8 kPa
ν (constant)	Pipe material Poisson's ratio	0.3
$\sigma_{y,1}, \epsilon_{p,1}, \sigma_{y,2}, \epsilon_{p,2}$ (constant)	Pipe material bilinear nonlinearity: yield stresses and plastic strains	$\sigma_{y,1} = 275000$ kPa, $\epsilon_{p,1} = 0$ $\sigma_{y,2} = 650000$ kPa, $\epsilon_{p,2} = 0.15$
ζ (constant)	Rayleigh damping	2%
H_s (constant)	Elevation of the mass centres of the two SDOF supporting structures in simplified models	5.3 m
a_g (constant)	Peak ground acceleration (PGA) of input ground motions	1.0 g

TABLE 2. List of earthquake records used as input ground motions

ID	Event	Station and recorded direction	unscaled PGA (g)	Predominant frequency f_g (Hz)
1	San Fernando (1971)	Santa Felita Dam (Outlet), 262	0.15	9.0
2	Northridge (1994)	Lake Hughes #9, 90	0.26	4.9
3	San Fernando (1971)	Castaic - Old Ridge Route, 21	0.32	3.0
4	Nicaragua (1972)	Managua ESSO, 90	0.26	2.2
5	San Fernando (1971)	Palmdale Fire Station, 120	0.11	1.2

List of Figures

715

716 1 Proposed structure-pipe-structure configuration: (a) Detailed 3D model, (b) simplified FE model of the
717 reference case, (c) illustration of varying H_p , (d) illustration of varying L_z , (e) illustration of varying L_x . 28

718 2 Illustration of acceleration time histories of Ricker wavelets with varying predominant frequencies. . . 29

719 3 $D_{diff,max}$ and $\epsilon_{h,max}$ responses with respect to variations of structural frequency ratio f_B/f_A and
720 predominant frequency of excitation f_g (Ricker wavelets for sub-figure (a) and (b); earthquake ground
721 motions for sub-figure (c) and (d)). Note the variation of f_B/f_A from 0.30 to 2.73 corresponds to
722 $f_A \equiv 3.3$ Hz and f_B varying from 1.0 Hz to 9.0 Hz. 30

723 4 Acceleration time histories (left) and their Fast Fourier Transform amplitudes (right) used as input
724 ground motions. PF: Predominant Frequency. 31

725 5 $D_{diff,max}$ and $\epsilon_{h,max}$ responses with respect to variations of H_p , K_A and K_B , L_z , L_x , as well as P . . 32

726 6 Substructuring scheme and key components of the HS. 33

727 7 Instrumentation: (a) strain gauges, (b) ovalization device. 34

728 8 $D_{diff}(t)$ responses (left) and force-displacement curves (right) obtained from the HS and the corre-
729 sponding FE prediction. The $D_{diff}(t)$ response of a no-pipe case is also plotted to reflect the impact
730 of structure-pipe-structure interaction. 35

731 9 $\epsilon_h(t)$ responses on four half-elbows of the HS and the corresponding FE prediction, obtained at the
732 significant strain location where maximum hoop strain occurred in FE prediction. 36

733 10 Pipe cross-sectional ovalization response: (a) Horizontal and vertical cross-sectional flattening versus
734 time curves on Elbow 2 from the HS and the corresponding FE prediction, (b) Horizontal and vertical
735 cross-sectional flattening versus D_{diff} curves on Elbow 2 from the HS and the corresponding FE
736 prediction. 37

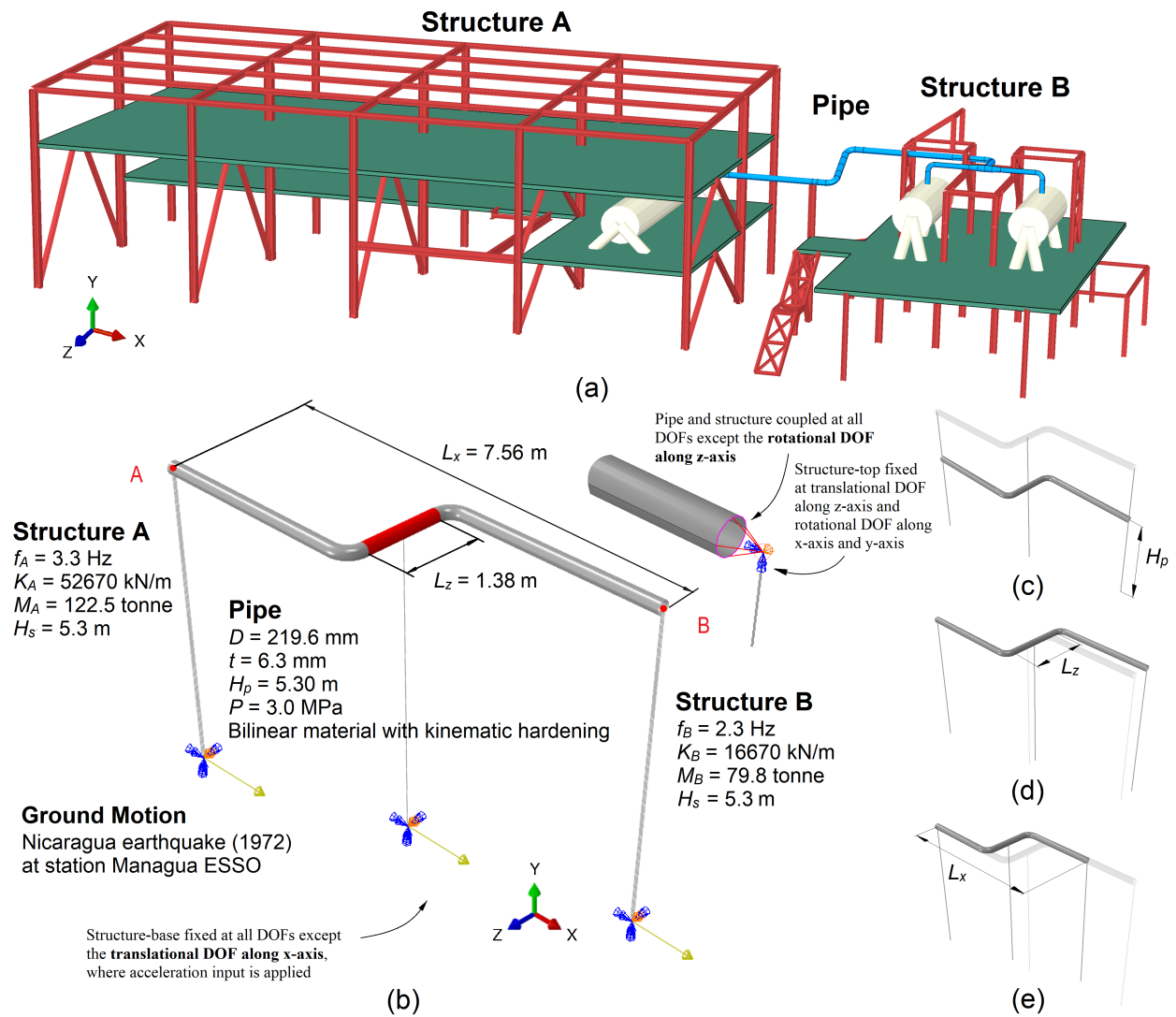


Fig. 1. Proposed structure-pipe-structure configuration: (a) Detailed 3D model, (b) simplified FE model of the reference case, (c) illustration of varying H_p , (d) illustration of varying L_z , (e) illustration of varying L_x .

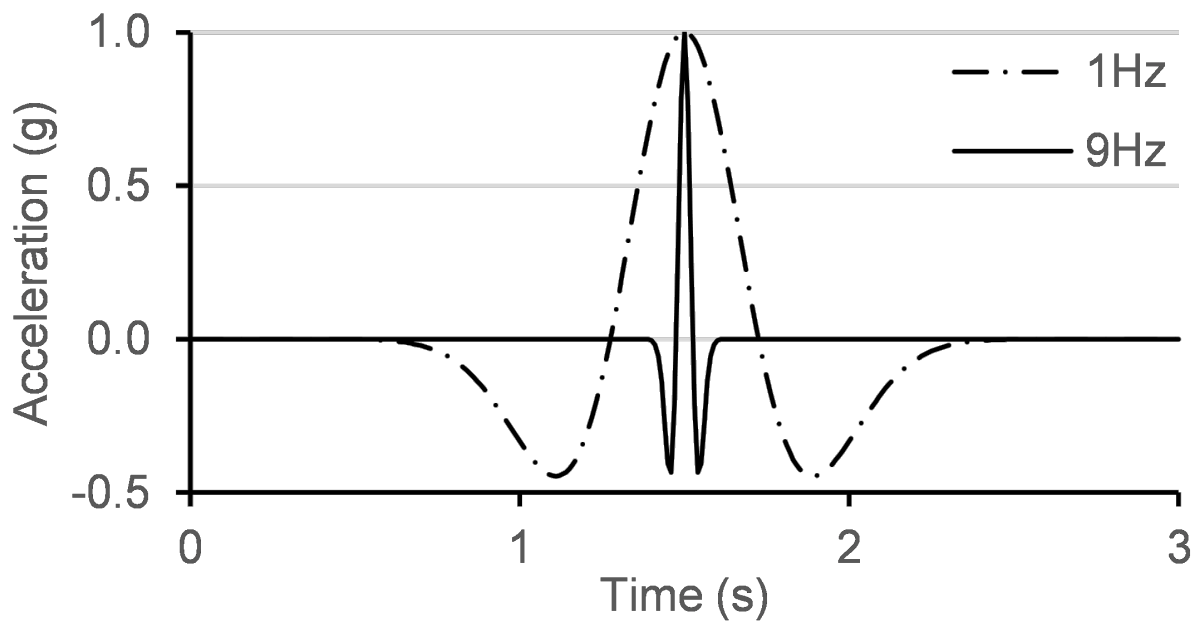


Fig. 2. Illustration of acceleration time histories of Ricker wavelets with varying predominant frequencies.

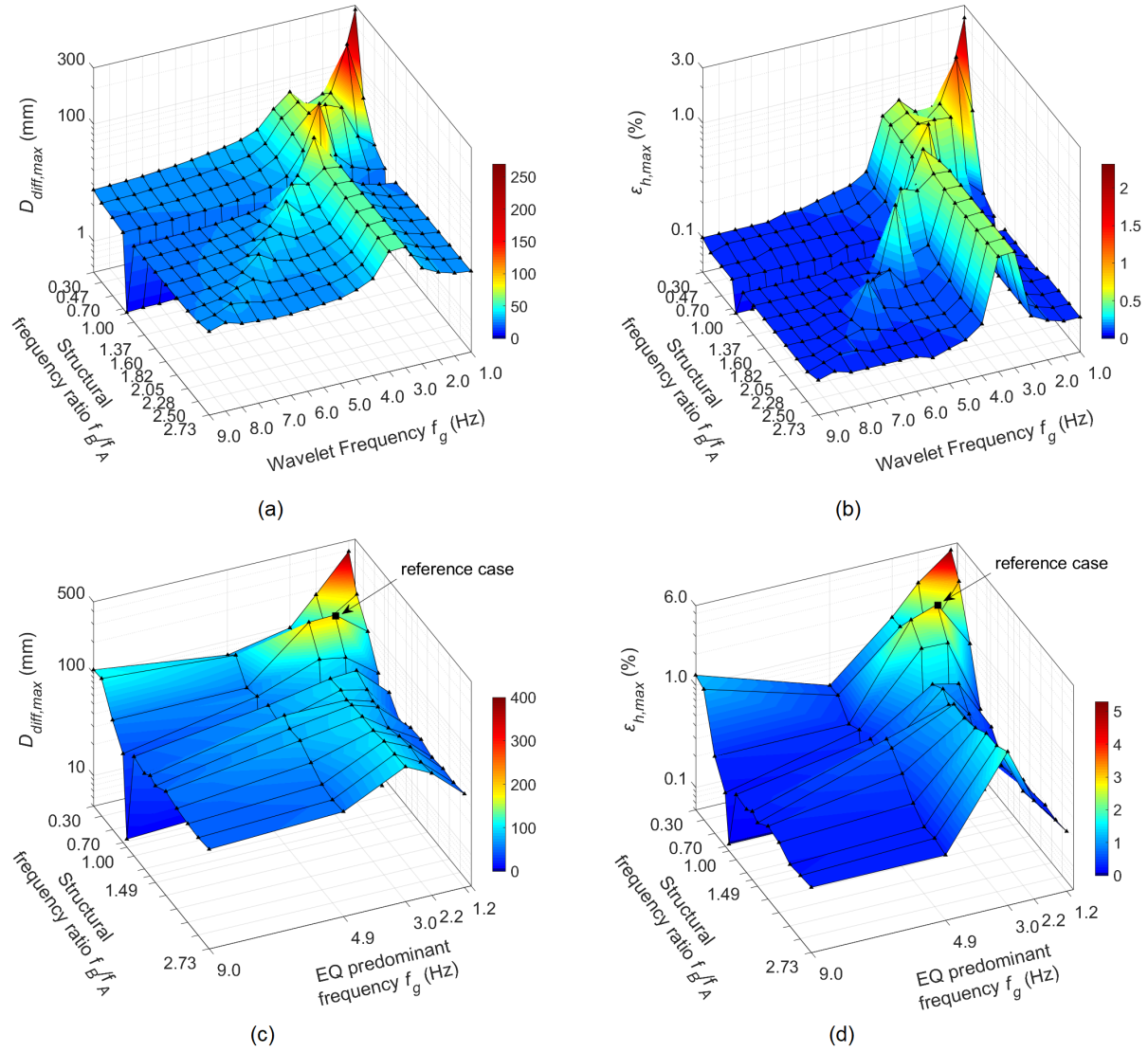


Fig. 3. $D_{diff,max}$ and $\epsilon_{h,max}$ responses with respect to variations of structural frequency ratio f_B/f_A and predominant frequency of excitation f_g (Ricker wavelets for sub-figure (a) and (b); earthquake ground motions for sub-figure (c) and (d)). Note the variation of f_B/f_A from 0.30 to 2.73 corresponds to $f_A \equiv 3.3$ Hz and f_B varying from 1.0 Hz to 9.0 Hz.

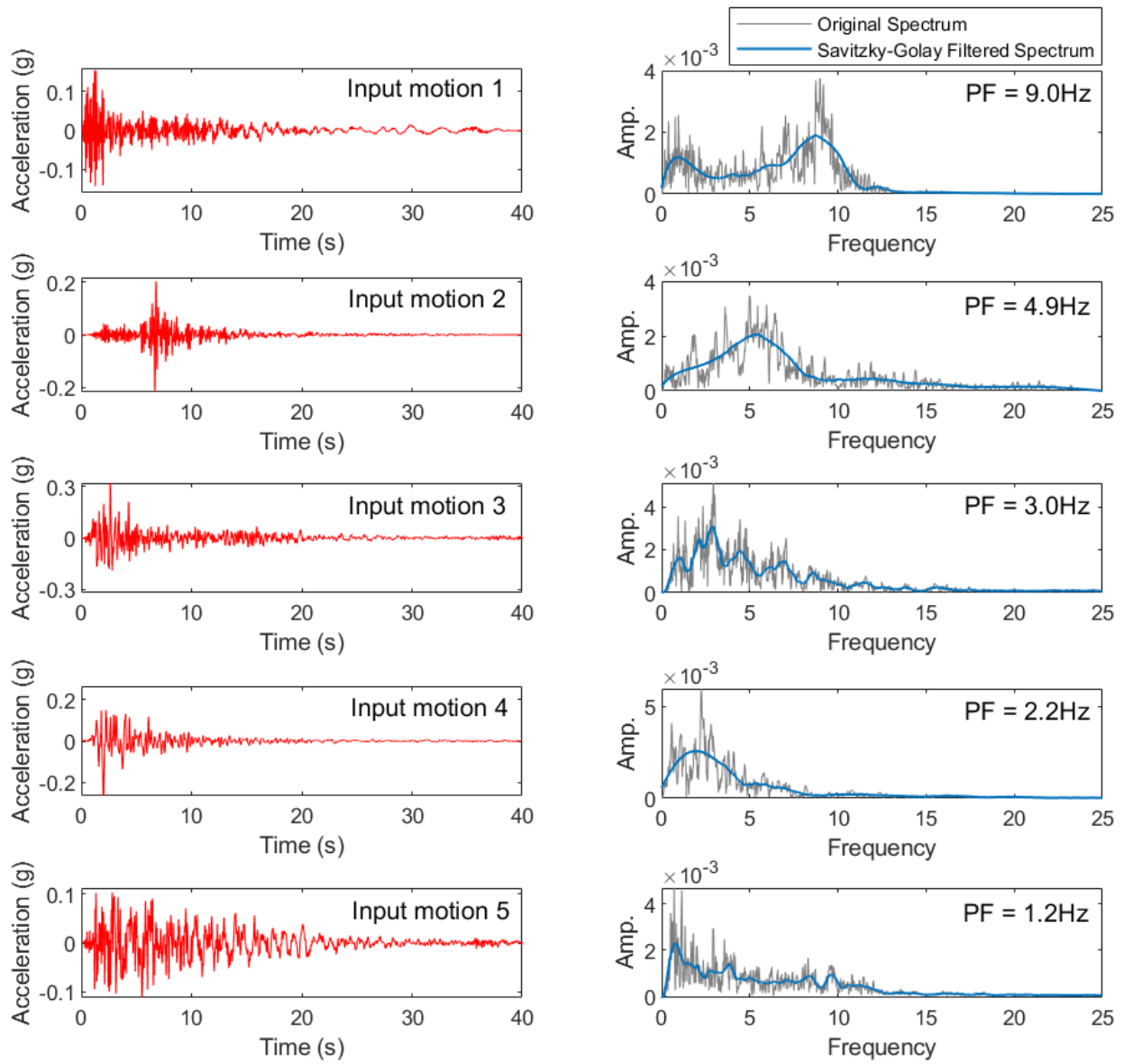


Fig. 4. Acceleration time histories (left) and their Fast Fourier Transform amplitudes (right) used as input ground motions. PF: Predominant Frequency.

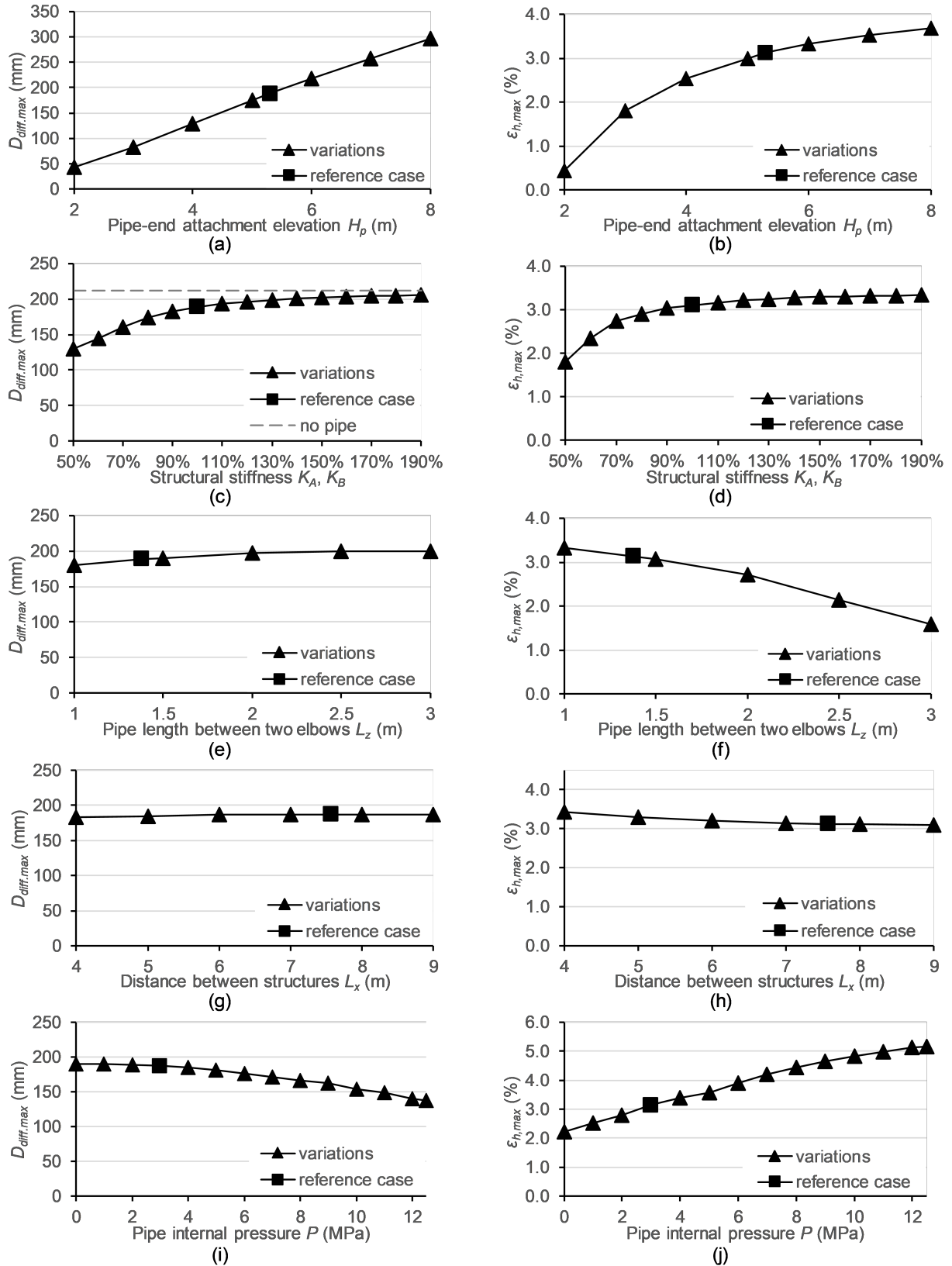


Fig. 5. $D_{diff,max}$ and $\epsilon_{h,max}$ responses with respect to variations of H_p , K_A and K_B , L_z , L_x , as well as P .

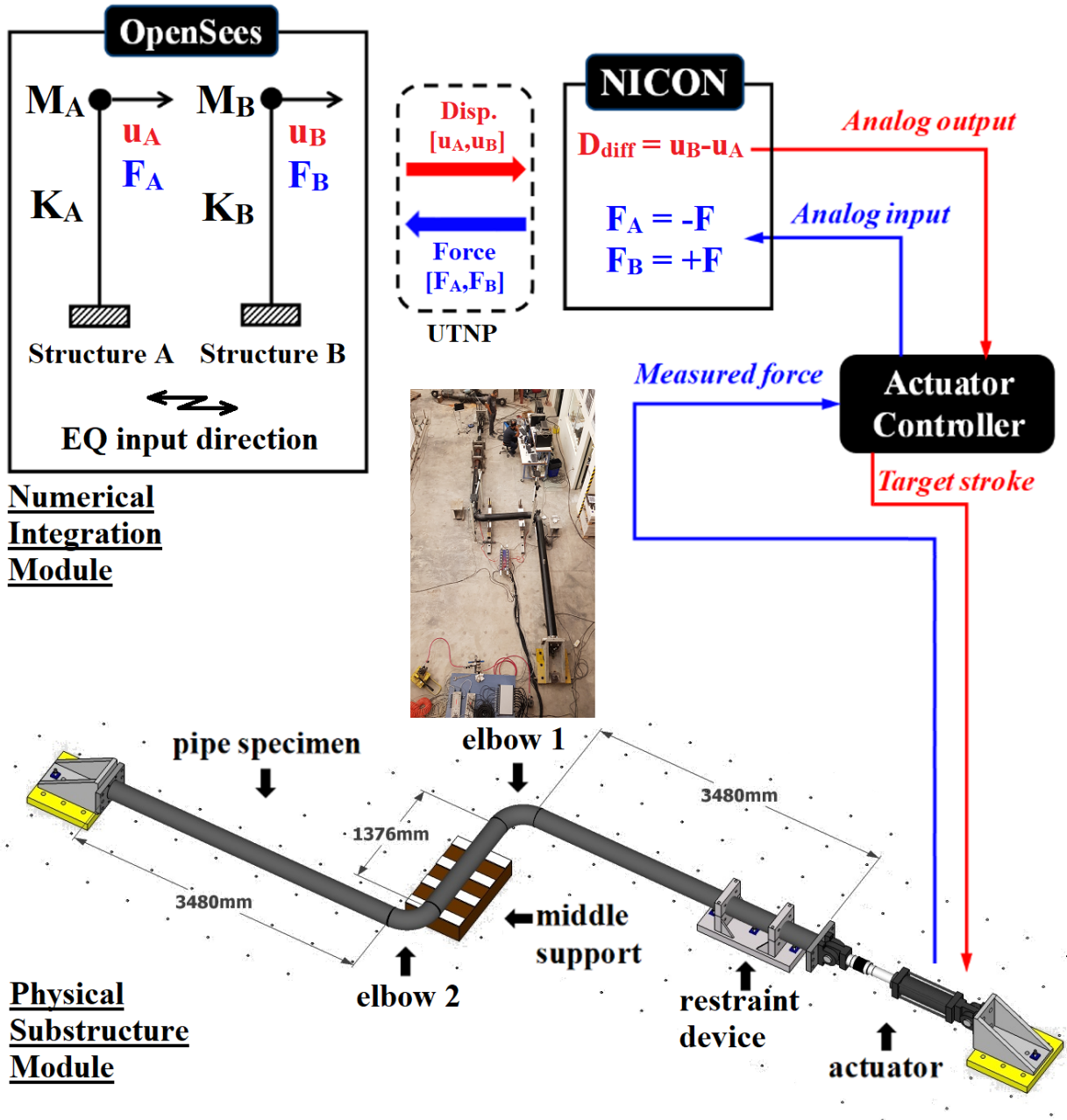


Fig. 6. Substructuring scheme and key components of the HS.

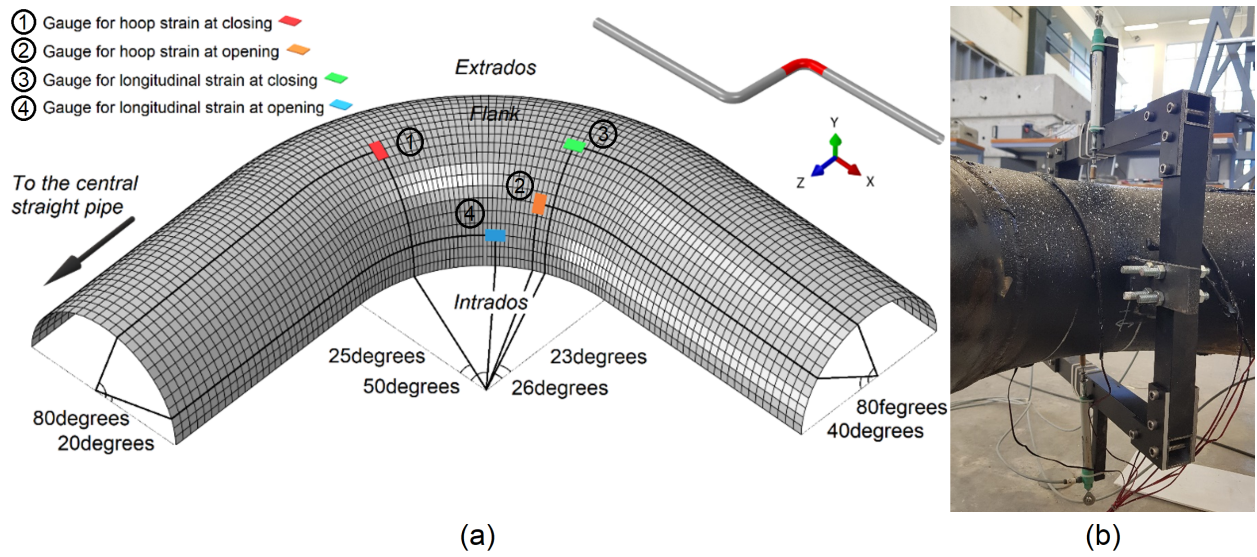


Fig. 7. Instrumentation: (a) strain gauges, (b) ovalization device.

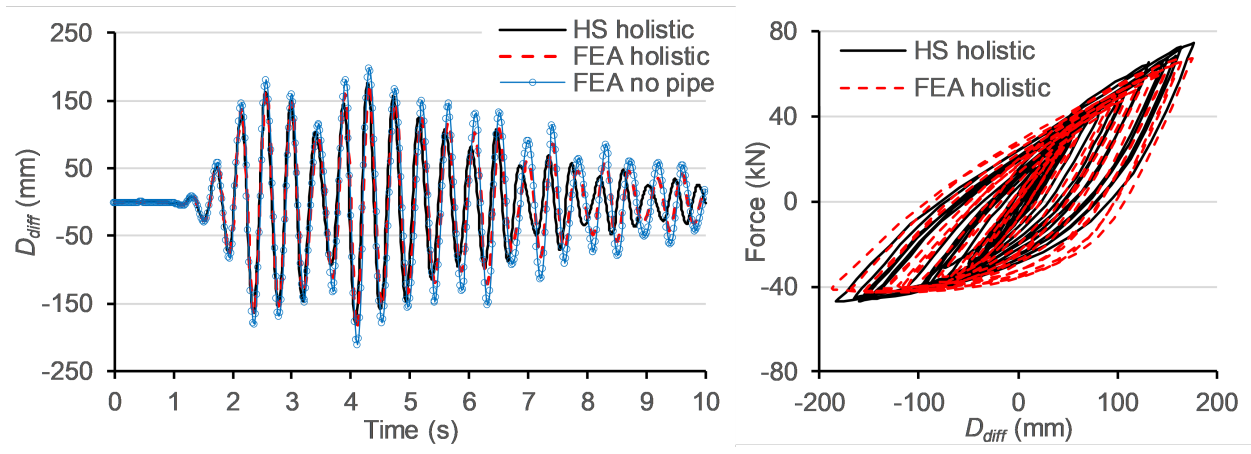


Fig. 8. $D_{diff}(t)$ responses (left) and force-displacement curves (right) obtained from the HS and the corresponding FE prediction. The $D_{diff}(t)$ response of a no-pipe case is also plotted to reflect the impact of structure-pipe-structure interaction.

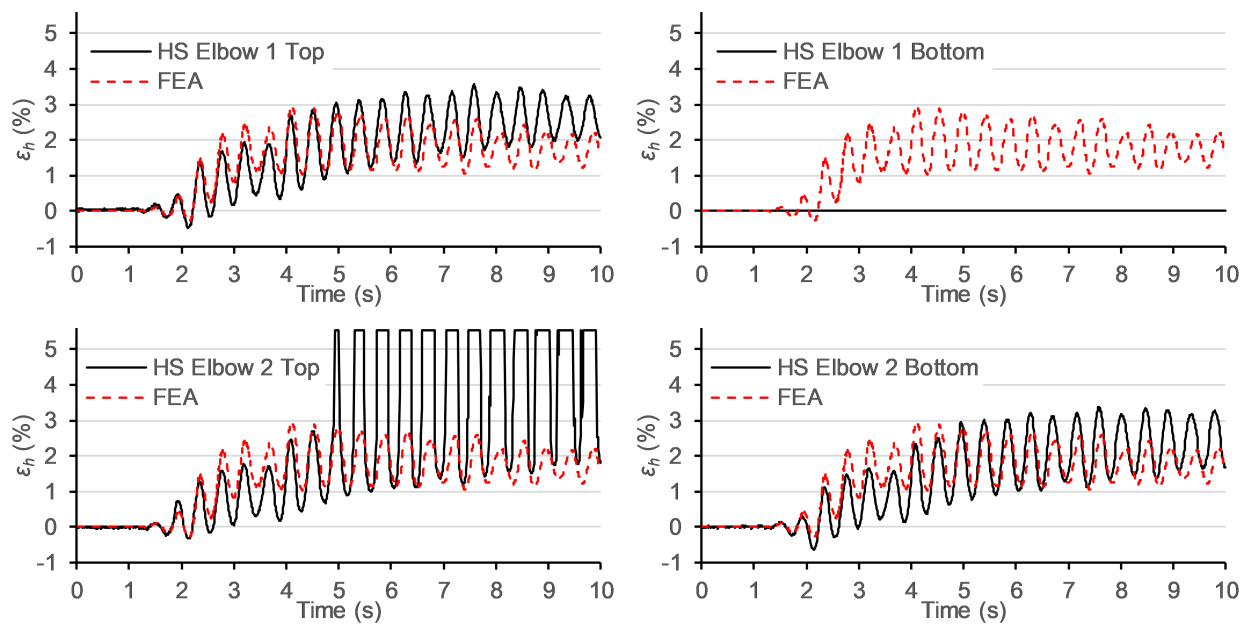


Fig. 9. $\epsilon_h(t)$ responses on four half-elbows of the HS and the corresponding FE prediction, obtained at the significant strain location where maximum hoop strain occurred in FE prediction.

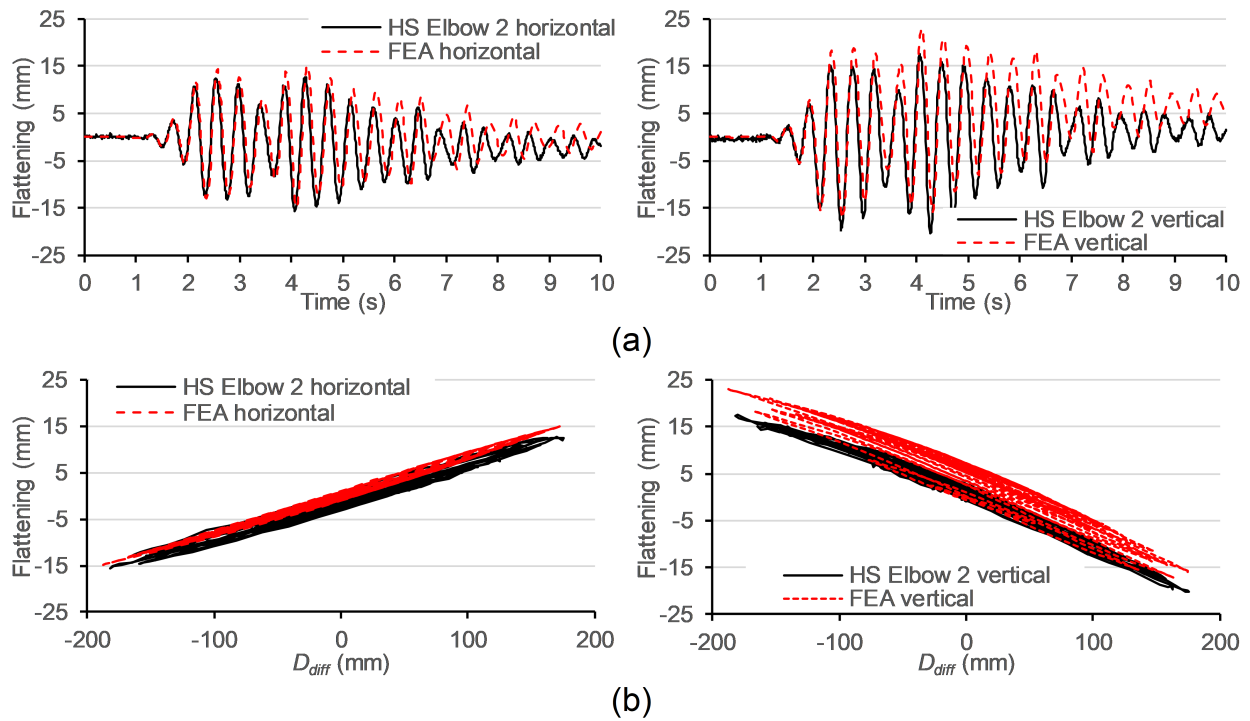


Fig. 10. Pipe cross-sectional ovalization response: (a) Horizontal and vertical cross-sectional flattening versus time curves on Elbow 2 from the HS and the corresponding FE prediction, (b) Horizontal and vertical cross-sectional flattening versus D_{diff} curves on Elbow 2 from the HS and the corresponding FE prediction.